








Hypomyelination, hypodontia and craniofacial abnormalities in a *Polr3b* mouse model of leukodystrophy

Mackenzie A. Michell-Robinson,^{1,2} Kristin E. N. Watt,³ Vladimir Grouza,^{1,4} Julia Macintosh,^{1,2} Maxime Pinard,⁵ Marius Tuznik,^{1,4} Xiaoru Chen,^{1,2} Lama Darbelli,^{1,2} Chia-Lun Wu,^{1,2}  Stefanie Perrier,^{1,2} Daryan Chitsaz,¹ Nonthué A. Uccelli,¹ Hanwen Liu,^{1,4}  Timothy C. Cox,⁶  Christoph W. Müller,⁷ Timothy E. Kennedy,¹ Benoit Coulombe,^{5,8} David A. Rudko,^{1,4,9}  Paul A. Trainor^{3,10} and  Geneviève Bernard^{1,2,11,12,13}

RNA polymerase III (Pol III)-related hypomyelinating leukodystrophy (POLR3-HLD), also known as 4H leukodystrophy, is a severe neurodegenerative disease characterized by the cardinal features of hypomyelination, hypodontia and hypogonadotropic hypogonadism. POLR3-HLD is caused by biallelic pathogenic variants in genes encoding Pol III subunits. While approximately half of all patients carry mutations in *POLR3B* encoding the RNA polymerase III subunit B, there is no *in vivo* model of leukodystrophy based on mutation of this Pol III subunit.

Here, we determined the impact of *POLR3B* Δ 10 (Δ 10) on Pol III in human cells and developed and characterized an inducible/conditional mouse model of leukodystrophy using the orthologous Δ 10 mutation in mice. The molecular mechanism of Pol III dysfunction was determined in human cells by affinity purification-mass spectrometry and western blot. Postnatal induction with tamoxifen induced expression of the orthologous Δ 10 hypomorph in triple transgenic *Pdgfra-Cre/ERT; R26-Stop^{fl}-EYFP; Polr3b^{fl}* mice. CNS and non-CNS features were characterized using a variety of techniques including microCT, *ex vivo* MRI, immunofluorescence, immunohistochemistry, spectral confocal reflectance microscopy and western blot. Lineage tracing and time series analysis of oligodendrocyte subpopulation dynamics based on co-labelling with lineage-specific and/or proliferation markers were performed.

Proteomics suggested that Δ 10 causes a Pol III assembly defect, while western blots demonstrated reduced *POLR3B* Δ 10 expression in the cytoplasm and nucleus in human cells. In mice, postnatal *Pdgfra*-dependent expression of the orthologous murine mutant protein resulted in recessive phenotypes including severe hypomyelination leading to ataxia, tremor, seizures and limited survival, as well as hypodontia and craniofacial abnormalities. Hypomyelination was confirmed and characterized using classic methods to quantify myelin components such as myelin basic protein and lipids, results which agreed with those produced using modern methods to quantify myelin based on the physical properties of myelin membranes. Lineage tracing uncovered the underlying mechanism for the hypomyelinating phenotype: defective oligodendrocyte precursor proliferation and differentiation resulted in a failure to produce an adequate number of mature oligodendrocytes during postnatal myelinogenesis.

In summary, we characterized the *Polr3b* Δ 10 mutation and developed an animal model that recapitulates features of POLR3-HLD caused by *POLR3B* mutations, shedding light on disease pathogenesis, and opening the door to the development of therapeutic interventions.

1 Department of Neurology and Neurosurgery, McGill University, Montréal, QC H3A 1A1, Canada

2 Child Health and Human Development Program, Research Institute of the McGill University Health Centre, Montréal, QC H4A 3J1, Canada

Received January 20, 2023. Revised June 23, 2023. Accepted July 06, 2023. Advance access publication August 28, 2023

© The Author(s) 2023. Published by Oxford University Press on behalf of the Guarantors of Brain.

This is an Open Access article distributed under the terms of the Creative Commons Attribution License (<https://creativecommons.org/licenses/by/4.0/>), which permits unrestricted reuse, distribution, and reproduction in any medium, provided the original work is properly cited.

- 3 Stowers Institute for Medical Research, Kansas City, MO 64110, USA
- 4 McConnell Brain Imaging Centre, Montreal Neurological Institute and Hospital, Montreal, QC H3A 2B4, Canada
- 5 Translational Proteomics Research Unit, Montreal Clinical Research Institute, Montréal, QC H2W 1R7, Canada
- 6 Department of Oral and Craniofacial Sciences, School of Dentistry, and Pediatrics, School of Medicine, University of Missouri – Kansas City, Kansas City, MO 64108, USA
- 7 Structural and Computational Biology Unit, European Molecular Biology Laboratory (EMBL), 69117 Heidelberg, Germany
- 8 Department of Biochemistry and Molecular Medicine, University of Montréal, Montréal, QC H3C 3J7, Canada
- 9 Department of Biomedical Engineering, McGill University, Montréal, QC H3A 2B4, Canada
- 10 Department of Anatomy and Cell Biology, The University of Kansas School of Medicine, Kansas City, KS 66160, USA
- 11 Department of Pediatrics, McGill University, Montréal, QC H4A 3J1, Canada
- 12 Department of Human Genetics, McGill University, Montréal, QC H4A 0C7, Canada
- 13 Department of Specialized Medicine, Division of Medical Genetics, Montreal Children's Hospital and McGill University Health Centre, Montréal, QC H4A 3J1, Canada

Correspondence to: Geneviève Bernard

Research Institute of the McGill University Health Centre, 1001 Boulevard Décarie, Block E

CHHD Mail Drop Point #EM03211 (Cubicle C), Montréal, QC H4A 3J1, Canada

E-mail: genevieve.bernard@mcgill.ca

Keywords: neurodevelopment; myelinogenesis; POLR3B; POLR3-related leukodystrophy; 4H leukodystrophy; mouse model

Introduction

POLR3-related hypomyelinating leukodystrophy (POLR3-HLD) is one of the most common hypomyelinating leukodystrophies. It is caused by biallelic pathogenic variants in genes encoding subunits of the RNA polymerase III (Pol III) complex; most commonly RNA polymerase III subunit A (POLR3A) and POLR3B, but also RNA polymerase I subunit C (POLR1C) and POLR3K.^{1–6} POLR3-HLD presents in previously healthy children in the first few years of life, leading to progressive disability and early death.⁷ The classic presentation includes hypomyelination, hypodontia and hypogonadotropic hypogonadism.^{7–10} While neurodegeneration is thought to be primarily driven by hypomyelination with secondary axonal loss, the disease pathogenesis is poorly understood.^{10–14} We hypothesize that Pol III hypofunction during a critical developmental period causes defective myelinogenesis and hypomyelination.¹⁵

Efforts to model POLR3-HLD *in vivo* using constitutive patient-derived mutations in POLR3A and POLR3B have been unsuccessful, owing either to a lack of phenotype or embryonic lethality.^{16,17} Recently, Merheb *et al.*¹⁸ developed an Olig2 conditional knock-in mouse model using a constitutively lethal double mutation in *Polr3a*.¹⁹ The model displays recessive characteristics including mild cerebral hypomyelination and neurobehavioral abnormalities but does not have gross motor defects, cerebellar hypomyelination, or non-neurological features.^{18,19} Because these are all typical features of the classic human disease, there was a clear need to develop and characterize a more representative disease model for developing therapeutic approaches in future preclinical studies. Nearly half of the patients with POLR3-HLD carry mutations in POLR3B and there is no working model of leukodystrophy based on that gene, so we elected to use *Polr3b* for our murine model.

Developing a leukodystrophy mouse model based on Pol III subunit mutations is not trivial. Constitutively-expressed mutations have not generated an appropriate level of phenotypic severity due to Pol III being necessary for survival during embryonic development.^{16–18} Fortunately, constitutively lethal mutations can be

expressed in a tissue- and/or time-dependent manner using Cre/lox technology to override the survival requirement for critical genes.^{18,20,21} An important question when developing such models is how a particularly severe mutant affects its milieu and the degree to which its effects resemble those of the disease one is attempting to replicate. Since we were interested in developing a leukodystrophy model based on a *Polr3b* mutation, it was important to make sure that the selected mutant impacted Pol III in a similar manner to patient-derived mutations.

Disease-causing mutations in Pol III subunits impact subunit expression/stability, Pol III biogenesis (complex assembly), nuclear import, and transcriptional activity.^{1,3,16,17,22,23} We became interested in a known *Polr3b* exon 10 deletion mutant ($\Delta 10$) because of its predicted impact on Pol III biogenesis.²⁴ The $\Delta 10$ mutant was discovered in a mutagenesis screen and initially described as the *polr3b* splice mutant *Slimjim* (Slj), which produces a gut phenotype in zebrafish.²⁴ To further understand the mutation, a mouse with a floxed exon 10 allele was generated for studying the gut using the Villin-Cre system, but was not evaluated in other tissues.²⁵ $\Delta 10$ has not specifically been detected in POLR3-HLD patients but POLR3B exon deletions have been reported,²⁶ as have missense (M243V, G244V, S268G) and nonsense/frameshift mutations in exon 10.^{8,10,27–31} Furthermore, intronic variants that alter splicing leading to exon skipping in the POLR3B transcript have been reported.^{8,10,29,32,33} Taken together, there was sufficient literature supporting the notion that both $\Delta 10$ and disease-causing POLR3B mutants had pathophysiological similarities at the gene and protein level, which made $\Delta 10$ an interesting candidate for further study in the context of POLR3-HLD.

We set out to characterize $\Delta 10$ at the molecular level in human cells in order to understand its effects on Pol III. Our proteomics studies suggested that $\Delta 10$ expression caused defective Pol III complex assembly, which was accompanied by reduced expression of the mutant protein in the cytosol and nucleus of human cells, like other known POLR3-HLD mutations.^{3,17} We then developed

an inducible/conditional expression model *in vivo*, whereby the orthologous $\Delta 10$ mutation was induced in a temporal and *Pdgfra*-dependent manner during early postnatal development in mice. Expressing $\Delta 10$ in this model led to recessive phenotypes, which were reminiscent of the cardinal manifestations of POLR3-HLD, including severe hypomyelination, hypodontia and craniofacial abnormalities. In-depth characterization of the CNS phenotype allowed us to answer fundamental questions about the development of severe hypomyelination in our model, such as whether the primary mechanism was reduced numbers of myelinating cells or reduced production of myelin by a normally sized pool of oligodendrocytes. We found that an early proliferation defect prevented the accumulation of adequate numbers of oligodendrocyte precursors, which was followed by a maturation defect in these precursors, suggesting that putative POLR3-HLD therapeutics will need to target oligodendrocyte precursors to correct hypomyelination.

Materials and methods

Detailed materials and methods for all sections are provided in the [Supplementary material](#).

Proteomics

DNA plasmids were constructed and cloned in p3XFLAG-CMV14 expression plasmids (Sigma). All plasmid sequences were verified by sequencing at each construction step. HEK293T cells (1.6×10^7) were transiently transfected for 24 h with 8.51 μg of plasmid containing human wild-type or mutant POLR3B in 15 cm plates using Jet Prime (PolyPlus) according to the manufacturer's recommended protocol. Cells were harvested, washed with $1 \times$ PBS, and snap frozen in liquid nitrogen. The FLAG affinity purification protocol was modified from Kean *et al.*³⁴ to produce samples for LC-MS/MS. High performance liquid chromatography (HPLC) was performed in a 75 μm i.d. \times 150 mm Self-Pack C18 column installed in the Easy-nLC II system (Proxeon Biosystems). HPLC was coupled to an Orbitrap Fusion mass spectrometer (Thermo Scientific) through a Nanospray Flex Ion Source (ThermoFisher, ES071). Label-free quantification (LFQ) intensity for each protein was obtained using MaxQuant (version 1.6.0.16) against the characterized human UniProtKB database (released on 3 June 2018).^{35,36} Log2 transformation, imputation and further statistical analysis were performed with Perseus (version 1.6.14.0).³⁷ All purifications were done in triplicate and proteins detected in all experiments were kept for further analysis. Missing values were replaced by randomly generated intensities normally distributed with a width of 0.3 times and a downshift of 1.8 times the standard deviation (SD) of non-zero intensities. Significant differences between Log2 protein intensities from bait purifications and the control groups were then determined using a two-tailed t-test subsequently adjusted for multiple hypothesis testing with a permutation-based false discovery rate (FDR) of 0.05 and an s_0 factor of 0.1 with 10 000 iterations. For all analyses, q -value ≤ 0.05 was considered statistically enriched.

Transgenic mice

Animal husbandry and all studies described in the publication including animal euthanasia adhered to our animal care and use protocol, as approved by the McGill University Health Centre Animal Resource Division (AUP8055). Parental strains used in the

study were *Pdgfra-Cre/ERT* ('*Pdgfra-CreERT*'),³⁸ *Polr3b^{fl}* (floxed exon 10)²⁵ and *R26-stop^{fl}-YFP* ('*YFP*').³⁹ Unless otherwise indicated, pups used in the study were generated from crosses between a *Pdgfra-CreERT*; *YFP*; *Polr3b^{+fl}* male and a *Polr3b^{fl/fl}* female. Tamoxifen-treatment induced conversion of unrecombined *Polr3b^{fl}* wildtype-equivalent allele into an exon 10 deletion allele, i.e. ' $\Delta 10$ '. Therefore, *Pdgfra-CreERT*; *YFP*; *Polr3b^{fl/fl}*, *Pdgfra-CreERT*; *YFP*; *Polr3b^{+fl}*, and *YFP*; *Polr3b^{fl/fl}* or *YFP*; *Polr3b^{+fl}* (Cre-negative control) mice were referred to as $\Delta 10/\Delta 10$, $+\Delta 10$ and CTRLs, respectively, when treated with tamoxifen. By convention, we have referred to mouse proteins in this article using title case (first letter capitalized) to differentiate them from human proteins (all capitals) without referring to species explicitly (e.g. Mbp versus MBP).

Tissue histology

Mice underwent transcardiac perfusion under isoflurane anaesthesia with PBS followed by a fixative for fresh frozen (FF) or formalin-fixed paraffin embedded (FFPE) block preparation. Tissues were harvested and sections prepared according to standard protocols for each method. Images of haematoxylin and eosin stained FFPE sections were acquired on a Leica Aperio AT Turbo digital whole slide scanning system at 20 \times resolution. Fluorescence images were acquired using a Zeiss AxioScan Z1 slide scanner employing a plan-apochromat 10 \times objective and AxioCam MR R3 camera.

Electrophoresis and immunoblotting

Brain tissue was prepared by dissection with hindbrain (cerebellum, pons, medulla) removed. Tissue lysates were prepared according to standard protocols in RIPA buffer with fresh protease inhibitors, normalized for protein concentration, and run on tris-glycine gels freshly prepared according to the Laemmli protocol with 0.5% trichloroethanol modification.⁴⁰ Activated proteins were transferred to PVDF support using the Bio-Rad Transblot Turbo, developed in Clarity Max enhanced chemiluminescence substrate, and imaged according to Bio-Rad manufacturer's protocols.

MRI

Paraformaldehyde (PFA)-fixed brains of 16 juvenile mice (P18) were used in this study. All imaging was performed using the Bruker Pharmascan 7 T pre-clinical MRI system. Multi-echo gradient-recalled-echo (mGRE) T_2^* -weighted image volumes were acquired using a 3D mGRE sequence with bipolar readout. Reconstructed 4D volumes were corrected for bipolar gradient induced misregistration and Gibbs ringing prior to calculation of myelin water fraction (MWF) images.^{41,42} Whole-brain MWF maps were calculated by fitting the three-pool relaxation model of white matter using a recently developed self-labelled encoder decoder (SLED) network implemented in PyTorch.^{43,44} Region of interest (ROI) parcellation was achieved by computing affine and symmetric diffeomorphic transformations between the mGRE volumes and an anatomically labelled reference atlas.⁴⁵

Cell counting

Histological images were exported from Zeiss proprietary format to full depth 16-bit tiff images in FIJI (ImageJ). Binary image masks were manually delineated in FIJI and saved as tiff images. Image processing pipelines were developed in CellProfiler 4.2.1 using representative images.^{46–50} Images and CellProfiler pipelines were exported to Amazon Web Services and imaging pipelines were run

using Distributed CellProfiler 2.0.0_4.1.3. The results were collated in SQLite databases and subsequently analysed in CellProfiler Analyst 3.0.4.

MicroCT

P18 mice were euthanized and stored in 95% ethanol until imaging. Mice were imaged at 15- μ m resolution using a Skyscan 1275 micro-computed tomography (microCT) scanner (Bruker). Raw scan data were reconstructed using NRecon and 3D rendered for visual assessment and measurement in Drishti v3.0 as previously described.⁵¹ All scans (55 kV, 0.5 mm Al filter, 45 ms exposure, 0.3° rotation step, four frame averaging), reconstruction and rendering settings were kept consistent between specimens.

Statistics

Statistical analyses were performed with GraphPad Prism 9.4.1 or SPSS v28 0.1.1 (IBM). Biological replicates are presented as individual points in all graphs unless otherwise indicated. For brevity, statistical analyses (tests), n , α , and other mathematical details pertaining to analysis and/or comparisons are detailed in the accompanying figure legends.

Results

Human $\Delta 10$ impairs Pol III complex assembly or stability

The mechanism by which $\Delta 10$ impacts Pol III function is unknown. We therefore endeavoured to characterize the $\Delta 10$ mutation in human cells to understand its impact on POLR3B protein expression as well as assembly and nuclear import of the mutant Pol III complex. First, we modelled the $\Delta 10$ mutation on the human Pol III cryo-EM structure and predicted that this deletion affects a central part of POLR3B (p.A242-Q282del).⁵² POLR3B exon 10 binds POLR3K and the jaw of POLR3A, suggesting that $\Delta 10$ would impair Pol III complex assembly or stability (Fig. 1A and B). To demonstrate this, POLR3B wild-type (WT) and $\Delta 10$ were cloned into separate 3XFLAG plasmids and transiently transfected into HEK293T cells. Anti-FLAG western blot analysis indicated that under identical conditions, 3XFLAG-POLR3B $\Delta 10$ (FLAG- $\Delta 10$) protein was not as highly expressed as 3XFLAG-POLR3B (FLAG-WT) protein (Fig. 1C), suggesting that FLAG- $\Delta 10$ (transcript or protein) is less stable than FLAG-WT. We next sought to determine if the FLAG- $\Delta 10$ protein could be found in nuclear extracts from plasmid-treated cells, as Pol III is assembled in the cytosol and imported to the nucleus for transcription. We detected FLAG in nuclear extracts at the expected molecular weight of FLAG- $\Delta 10$, demonstrating that FLAG- $\Delta 10$ was able to form complexes competent for import (Fig. 1D). Using affinity purification coupled to mass spectrometry (AP-MS), we were able to determine, by comparing the POLR3B $\Delta 10$ mutant to the negative control FLAG alone, that some Pol III subunits were absent from the 3XFLAG-POLR3B $\Delta 10$ complex (Fig. 1E), as summarized by the model shown in Fig. 1F. Our findings verified that $\Delta 10$ expression impaired Pol III complex assembly or stability and reduced POLR3B protein expression in human cells.

Developing a *Pdgfra*-dependent $\Delta 10$ expression model *in vivo*

POLR3B mutations resulting in Pol III complex assembly defects are known to be causal in POLR3-HLD.¹⁷ Therefore, we elected to study the $\Delta 10$ mutation *in vivo* in the context of oligodendrocyte precursor

cell (OPC) development using an inducible/conditional *Pdgfra*-CreERT system. To target $\Delta 10$ expression to the largest group of OPCs possible without toxicity, we validated a postnatal tamoxifen injection protocol in control mice. Dosing trials on wild-type animals (Supplementary Fig. 1A) allowed us to select daily injections of tamoxifen at 40 mg/kg from P2–P5 as our dosing regimen.

By crossing the *Pdgfra*-CreERT and YFP founder strains, we generated double heterozygous control mice and assessed tamoxifen recombination efficiency. Administration of tamoxifen according to the protocol defined above demonstrated that 55–98% of Olig2+ cells were also YFP+ at P9, depending on the brain region. All regions analysed except the cortex maintained a recombination efficiency of over 55% until P21 (Supplementary Fig. 1B). This experiment also independently validated that the *Pdgfra*-CreERT allele produced high-fidelity recombination in the oligodendrocyte lineage, as >90% of YFP+ cells were also Olig2+ in histological sections at P9 and P14 with expected recombination also observed in capillary endothelium and choroid plexus (not shown).³⁸

We developed a *Pdgfra*-CreERT; YFP; *Polr3b* triple transgenic model to express $\Delta 10$ and YFP in *Pdgfra*+ cells. Genotyping PCRs and validation sequencing of the founder strains yielded the expected results (Supplementary Fig. 1C–E).^{25,38,39} In <5% of total live births, we detected germ line transmission of a $\Delta 10$ allele by PCR. Pups with germ-line recombination were screened out of subsequent studies. Brain recombination was validated by genotyping PCR using tissue from *Pdgfra*-CreERT; *Polr3b*^{+/^{fl}} and *Pdgfra*-CreERT; *Polr3b*^{fl/^{fl}} double transgenic mice (Supplementary Fig. 1F). Expression of the $\Delta 10$ mRNA was subsequently validated by RT-PCR in tamoxifen-treated +/ $\Delta 10$ mice (P30), and the products were sequenced confirming the integrity of the exon 9–11 boundary in spliced mRNA. All subsequent studies were carried out with triple transgenic mice.

Pdgfra-dependent $\Delta 10$ expression produces recessive phenotypes consistent with POLR3-HLD

In $\Delta 10/\Delta 10$ mice, phenotypic differences from +/ $\Delta 10$ and CTRL mice became apparent starting at P11/12. Behaviourally, $\Delta 10/\Delta 10$ mice displayed a neurological phenotype including ataxia, tremor and spontaneous seizures (Supplementary Videos 1–4). $\Delta 10/\Delta 10$ size differences also became apparent in the second week of life as they remained smaller than littermates. $\Delta 10/\Delta 10$ mice had significantly reduced body size and weight at the P21 end point, which underscored their abnormal developmental trajectory in the second and third weeks of life (Fig. 2A and B). The median survival of $\Delta 10/\Delta 10$ mice was 24 days, and all perished by 26 days ($n=43$), whereas +/ $\Delta 10$ ($n=72$) and CTRL ($n=116$) mice had adequate and comparable survival (Fig. 2C). Approximately 15% of +/ $\Delta 10$ and CTRL mice were lost to the gestalt effects of tamoxifen and/or maternal neglect from significant perinatal handling (Fig. 2C). More detailed behavioural analysis and quantification were not done due to the small size, poor health and early lethality in $\Delta 10/\Delta 10$ mice.

$\Delta 10/\Delta 10$ mice also had craniofacial and dental anomalies, consistent with POLR3-HLD but unique among leukodystrophy mouse models (Fig. 2D). All $\Delta 10/\Delta 10$ mice had absent incisors or delayed eruption of underdeveloped incisors, whereas +/ $\Delta 10$ and CTRL had normal tooth eruption/development (Table 1). High resolution microCT of the craniofacial bones and teeth (Fig. 2E–M) confirmed that $\Delta 10/\Delta 10$ mice had smaller/hypoplastic incisors with/without eruption (Fig. 2E–G) whereas molars appeared normal. Some +/ $\Delta 10$ and all $\Delta 10/\Delta 10$ exhibited posterior frontal (metopic) suture anomalies, suggestive of increased pressure from constrained

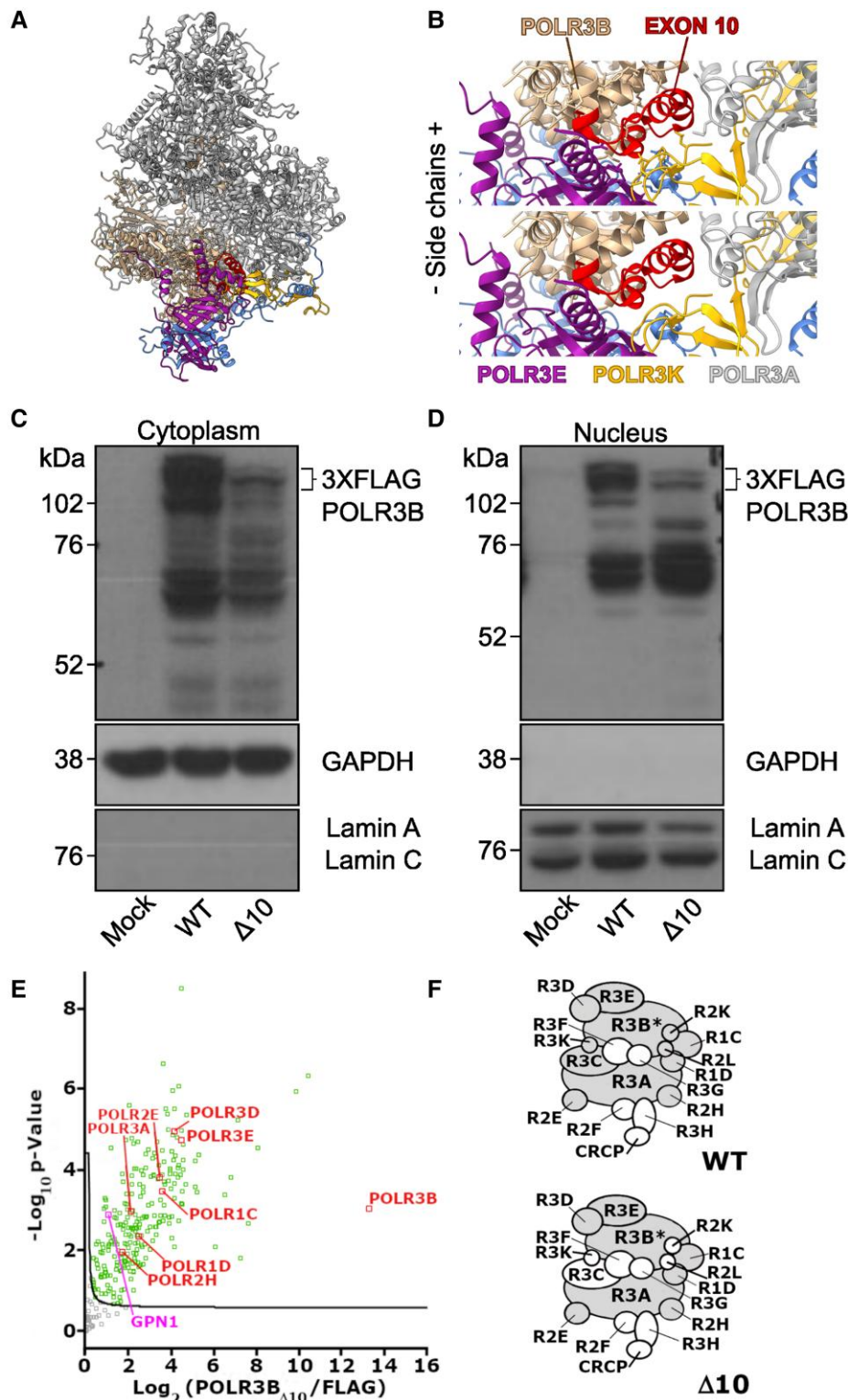


Figure 1 POLR3B exon 10 deletion impairs Pol III assembly or stability in human cells. (A) Human Apo Pol III structural model. (B) Human Apo Pol III rotated and zoomed with POLR3B exon 10 highlighted in red and nearby subunits labelled including heterodimer subunit POLR3E, POLR3K and POLR3A (jaw). (C) Representative anti-FLAG western blot of cytoplasmic extract from HEK293T cells transiently transfected with p3XFLAG (mock), wild-type POLR3B-FLAG (WT) or POLR3B Δ 10-FLAG (Δ 10) for 24 h. Loading controls for the cytoplasmic (GAPDH) and nuclear (Lamin A, C) fractions are shown. (D) Representative anti-FLAG western blot of nuclear extract from HEK293T cells transiently transfected with p3XFLAG (mock), wild-type POLR3B-FLAG (WT) or POLR3B Δ 10-FLAG (Δ 10) for 24 h. Loading controls for the cytoplasmic (GAPDH) and nuclear (Lamin A, C) fractions are shown. (E) Volcano plot illustrating the log₂-transformed average label-free quantification (LFQ)-intensity difference between the Δ 10 mutant against the FLAG expressing control (x-axis). The significantly different Pol III subunits are marked in red and the significantly different GPN cofactors in pink. Other proteins marked in green are considered significantly different. (F) Schematic representation showing significantly different subunits evaluated by AP-MS. Wild-type data from Djordjevic et al.⁵³ were used to show expected Pol III subunits. Subunits that are significantly increased compared to their FLAG control are marked in grey. Subunits that are not detected or not significantly different from the FLAG control are marked in white. *The subunit used as bait.

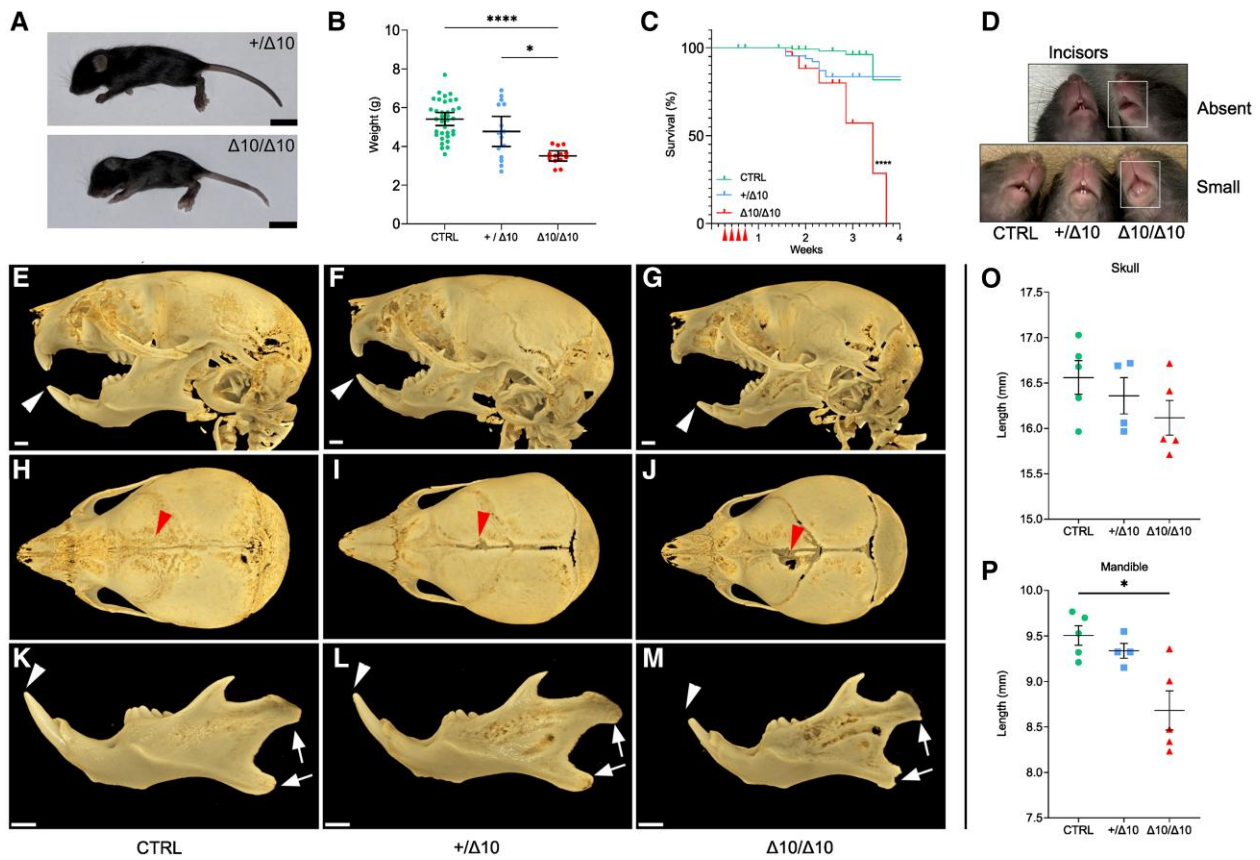


Figure 2 $\Delta 10$ homozygous mice have reduced size and survival, as well as abnormal craniofacial development. (A) Representative size difference between $+/ \Delta 10$ (top) and $\Delta 10 / \Delta 10$ (bottom) littermates (Scale bar = 1 cm). (B) Weight of transgenic mice at the P21 end point where each point represents an individual mouse weight, including $n = 13 \Delta 10 / \Delta 10$, $n = 15 + / \Delta 10$ and $n = 35$ CTRL mice. (C) Kaplan-Meier plot of survival of $\Delta 10 / \Delta 10$ ($n = 43$) versus $+/ \Delta 10$ ($n = 72$) and CTRL ($n = 116$). Median survival in $\Delta 10 / \Delta 10$ was 24 days. Comparison of the survival curves and statistical significance were evaluated by Log-rank (Mantel-Cox) test ($P < 0.0001$). (D) Top: representative image of littermates where the $\Delta 10 / \Delta 10$ (right) has apparent absence of incisors at P21. Bottom: representative image of three littermates where the $\Delta 10 / \Delta 10$ (right) has small incisors at P21. (E–M) MicroCT analysis of $\Delta 10 / \Delta 10$ mice at P18 demonstrated dental and craniofacial anomalies. (E–G) Lateral views demonstrate hypoplastic incisors (white arrowheads) and mandibles in $\Delta 10 / \Delta 10$. (H–J) Dorsal views show deficiencies in the frontal bone (red arrowheads) in $\Delta 10 / \Delta 10$ mice relative to $+/ \Delta 10$ and CTRL. The skull length tends to be shorter in homozygous mice relative to controls (see O, below), but the differences were not statistically significant. (K–M) Isolated mandibles demonstrate general hypoplasia and an abnormal condylar head and mandibular angle shape (white arrows). (O and P) The incisors (white arrowheads) are small, and the length of the mandible is significantly shorter in homozygous mutants relative to controls. (O) Quantification of skull length, with biological replicates plotted as individual points. (P) Quantification of mandible length, with biological replicates plotted as individual points. The P-values in the plots in O and P were determined using Brown-Forsythe and Welch one-way ANOVA followed by multiple comparisons testing using the Dunnett T3 method with $\alpha = 0.05$. Scale bar = 1 mm. * $P < 0.05$, ** $P < 0.01$, *** $P < 0.001$, **** $P < 0.0001$. POLR3B-HLD = RNA polymerase III subunit B-related hypomyelinating leukodystrophy; $\Delta 10 / \Delta 10$ = tamoxifen-treated transgenic mice carrying a *Pdgfra-CreERT* allele and homozygous *Polr3b^{fl}* alleles; $+/ \Delta 10$ = tamoxifen-treated transgenic mice carrying a *Pdgfra-CreERT* allele and heterozygous *Polr3b^{fl}* alleles; CTRL = tamoxifen-treated transgenic mice carrying no *Pdgfra-CreERT* allele(s).

growth of the midface (Fig. 2H–J). $\Delta 10 / \Delta 10$ had rounder appearing heads and their mandibular condyle and angle were overtly dysmorphic (Fig. 2H–M). $\Delta 10 / \Delta 10$ mice tended to have smaller skulls (Fig. 2H–J) and mandibles (Fig. 2K–M) compared to CTRL, but differences between $\Delta 10 / \Delta 10$ and $+/ \Delta 10$ were not statistically significant (Fig. 2O and P). These apparent size differences were proportional to body weight/size.

Myelin basic protein immunofluorescence revealed hypomyelination in $\Delta 10$ homozygotes

To understand whether $\Delta 10$ mice have a deficit in myelin development, we examined brain tissue for myelin basic protein (Mbp). On macroscopic inspection, $\Delta 10 / \Delta 10$ brains had less visible ventral myelin, but overall tissue morphology was normal based on haematoxylin and eosin staining (Supplementary Fig. 2). However,

immunofluorescence staining of fixed-frozen tissue collected at P9, P14 and P18 in CTRL, $+/ \Delta 10$, and $\Delta 10 / \Delta 10$ mice indicated significant hypomyelination. In P9 sagittal sections, Mbp expression was slightly reduced in $\Delta 10 / \Delta 10$ s, but the overall state of myelination appeared similar between $+/ \Delta 10$ s and $\Delta 10 / \Delta 10$ s (Fig. 3A). By P14, Mbp expression had developed in the midbrain and forebrain of $+/ \Delta 10$ s and CTRLs whereas in $\Delta 10 / \Delta 10$ s, development had not progressed. By P18, midbrain and forebrain Mbp expression were further increased in $+/ \Delta 10$ s/CTRLs, whereas expression had not advanced significantly in $\Delta 10 / \Delta 10$ s (Fig. 3A). We noted development of sparse Mbp expression in the corpus callosum and striatum in $\Delta 10 / \Delta 10$ s (Fig. 3B). In the cervical spinal cord, Mbp expression was also impacted, primarily in the ventral horn (Fig. 3C). Taken together, we observed an abnormal developmental progression of myelin antigen expression in the second and third weeks of life in $\Delta 10 / \Delta 10$ s (Fig. 3 and Supplementary Fig. 3).

Table 1 Hypodontia frequency in the *Polr3b*-HLD mouse model

<i>Polr3b</i> status	Incisor size at end point (n)			Total
	Normal	Small	Absent	
$\Delta 10/\Delta 10$	0*	6*	9*	15
$+\Delta 10$	22	0	0	22
CTRL	41	0	0	41

The appearance of the incisors was categorized and counted at terminal end points (P14–P34) in 14 litters of $\Delta 10/\Delta 10$, $+\Delta 10$ and CTRL mice. Frequencies in each incisor size group are categorized by genotype. Normal incisors were defined as incisors that were the same length as CTRL littermates. Small incisors were defined as being less than half the length of the incisors of a CTRL littermate. Absent incisors were categorized when incisors had not visibly erupted. Male and female $\Delta 10/\Delta 10$ mice had similar frequencies of absent incisors (5/8 females, 4/7 males) and small incisors (3/8 females, 3/7 males). In a sex-pooled statistical analysis, $\Delta 10/\Delta 10$ mice had a significantly smaller proportion of mice with normal incisors and greater proportion of mice with either small or absent incisors, as compared to $+\Delta 10$ s and CTRLs. Statistical analysis of incisor size and sex did not indicate dependence of these variables (not shown). Statistical significance was computed by cross-tabulation of genotype and incisor size using a Fisher-Freeman-Halton Exact test in SPSS v28.0.0.1 (IBM). The Fisher-Freeman-Halton Exact Test indicated a statistically significant association between genotype and incisor size (64.239, exact two-sided significance <0.001). The proportion of mice in an incisor size group were categorized by genotype using the Z-test of independent proportions with significance tested post hoc adjusting for multiple comparisons by the Bonferroni method ($\alpha = 0.05$). Using this method, differences in the proportion of $\Delta 10/\Delta 10$ s with normal, small, or absent incisors were evaluated as statistically different from the corresponding proportion in $+\Delta 10$ and CTRL mice. POLR3B-HLD = RNA polymerase III subunit B-related hypomyelinating leukodystrophy; $\Delta 10/\Delta 10$ = tamoxifen-treated transgenic mice carrying a *Pdgfra*-CreERT allele and homozygous *Polr3b^{fl}* alleles; $+\Delta 10$ = tamoxifen-treated transgenic mice carrying a *Pdgfra*-CreERT allele and heterozygous *Polr3b^{fl}* alleles; CTRL = tamoxifen-treated transgenic mice carrying no *Pdgfra*-CreERT allele(s).

*P < 0.05.

Quantifying hypomyelination severity in $\Delta 10$ homozygotes

We performed detailed studies to quantify the putative hypomyelination in our transgenic model at P18, including MRI. Assessment of the MWF using *ex vivo* MRI techniques on PFA-fixed brains from P18 mice revealed visible differences in MWF maps indicative of significant hypomyelination in $\Delta 10/\Delta 10$ s, in addition to a substantial effect of tamoxifen on myelination overall (Supplementary Fig. 4A–G). Overall myelination status at the group level was described in aggregate by taking the summed average MWF values from seven ROIs (Supplementary Fig. 4F and G). Representative MWF maps are shown in Fig. 4A. Quantitative comparison of $+\Delta 10$ and $\Delta 10/\Delta 10$ aggregate MWF revealed a statistically significant decrease in myelination in $\Delta 10/\Delta 10$ s relative to $+\Delta 10$ s (Fig. 4B).

To better understand the degree of hypomyelination, we pursued both spectral confocal reflectance (SCoRe) microscopy (Fig. 4C), a label-free technique for imaging myelin⁵⁴ and traditional myelin staining with Luxol Fast Blue (LFB) (Supplementary Fig. 5). At P18, both methods demonstrated reduced myelination in $\Delta 10/\Delta 10$ s compared to littermates. More specifically, statistically significant reductions in mean SCoRe area were observed in the corpus callosum (Fig. 4D), cerebellum (Fig. 4F) and brainstem (Fig. 4G) of $\Delta 10/\Delta 10$ s relative to $+\Delta 10$ s. Both MRI and histological techniques agreed with our Mbp expression studies that hypomyelination was well established by P18.

Finally, we confirmed the amount of protein expression in the midbrain/forebrain by performing western blots using midbrain/forebrain lysates from male and female mice at P21 (Fig. 4H).⁵⁵

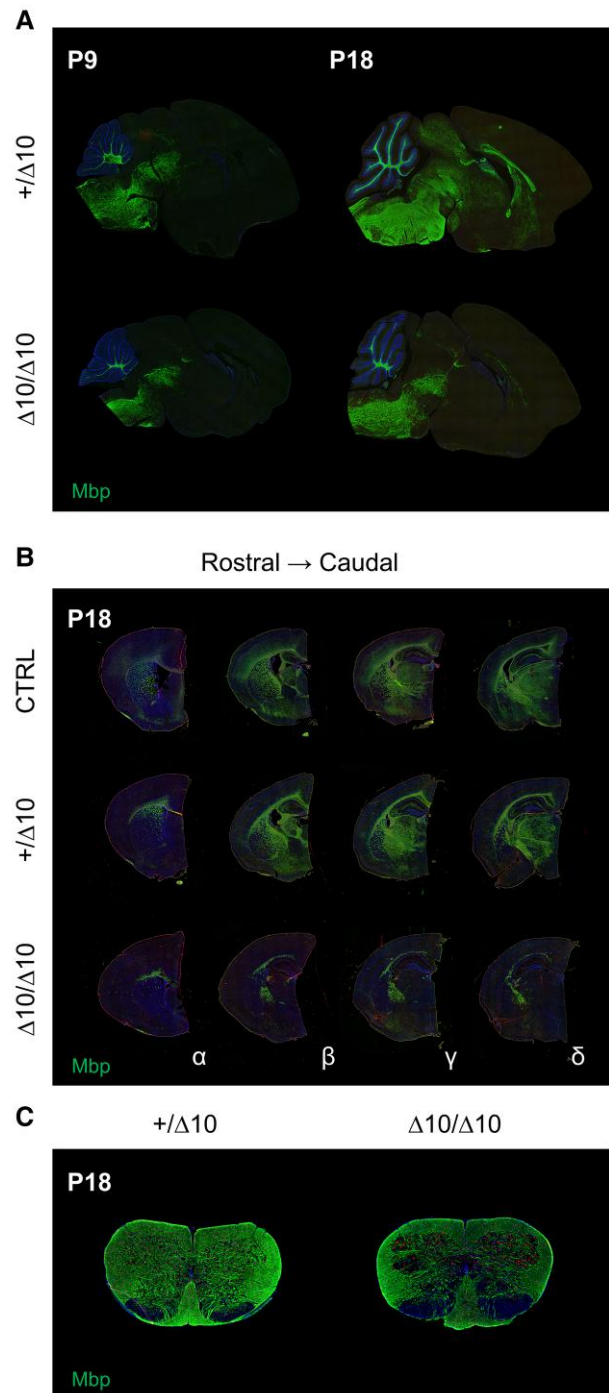


Figure 3 Midbrain and forebrain myelinogenesis is interrupted between P9 and P18 in $\Delta 10$ homozygous mice. (A) Mbp expression (green) in parasagittal sections from $+\Delta 10$ (top) and $\Delta 10/\Delta 10$ (bottom) demonstrate interruption of myelinogenesis in the midbrain and forebrain between P9 and P18 in $\Delta 10/\Delta 10$. (B) Mbp expression (green) in hemicoronal sections from CTRL, $+\Delta 10$ (left) and $\Delta 10/\Delta 10$ at P18. Four levels of sections (alpha, beta, gamma, delta) were cut from hemi-coronal blocks in order to assess Mbp expression via immunofluorescence. These four levels of sections correspond to the quantification found in Supplementary Fig. 3B. (C) Mbp expression in the cervical spinal cord at P18 demonstrates a relative reduction in ventral cord myelination between $+\Delta 10$ (left) and $\Delta 10/\Delta 10$ (right). Reduced grey matter Mbp expression is also apparent in $\Delta 10/\Delta 10$. POLR3B-HLD = RNA polymerase III subunit B-related hypomyelinating leukodystrophy; $\Delta 10/\Delta 10$ = tamoxifen-treated transgenic

(continued)

Our assays included Polr3a, Polr3b, Pdgfra, Ng2, Olig2 and Mbp. Among these, Ng2 was on trend for increased expression in $\Delta 10/\Delta 10$ s, while Olig2 and Mbp were negatively correlated with $\Delta 10$ allele dose (Fig. 4I–K). We observed statistically significant reductions in both Olig2 (Fig. 4J) and Mbp (Fig. 4K) expression in $\Delta 10/\Delta 10$ s relative to $+/ \Delta 10$ s. We ran age-matched homozygous shiverer tissue lysates as a negative control next to samples from $\Delta 10/\Delta 10$ mice and found the Mbp western blot quantification results to be indistinguishable. Our tissue biochemistry results quantified significant hypomyelination in the midbrain/forebrain of $\Delta 10/\Delta 10$ mice.

$\Delta 10$ homozygotes produce fewer oligodendrocyte precursors, reducing the number of myelinating cells

To ascertain whether there were differences in subpopulations of oligodendrocyte lineage cells (OLCs) that might explain the observed hypomyelination, we conducted YFP+ lineage tracing on histological sections using antibodies against lineage marker antigens. We quantified cells based on the expression of markers of OPCs (Pdgfra+ and/or Ng2+) or mature oligodendrocytes (OL; Apc clone CC1+). We investigated hindbrain, midbrain and forebrain structures at P9, P14 and P18 (Supplementary Figs 6 and 7). At P9, YFP+Pdgfra+ OPCs were present throughout parasagittal brain sections (Fig. 5A and B), as were YFP+Ng2+ OPCs (Fig. 5C and D), and the total numbers of CC1+ OLs were equivalent between groups, making it an ideal time point to begin to study OLC population dynamics leading up to the period of peak myelination in mice.

Cell counting indicated steadily reduced numbers of OPCs and OLs over the P9–P18 window in $\Delta 10/\Delta 10$ s (Fig. 6). We analysed both single positive cells and cells co-expressing markers in addition to YFP. Single positive Pdgfra+ or CC1 cells and cells co-expressing these markers in addition to YFP, showed similar population dynamics in $+/ \Delta 10$ s and CTRLs suggesting that tissue-level OLC population dynamics were relatively normal in $+/ \Delta 10$ s. By comparison, in $\Delta 10/\Delta 10$ s, OLC populations decreased in number over time (Fig. 6B and C). $+/ \Delta 10$ s and CTRLs demonstrated an increase in the ratio of OLs (CC1+) to OPCs (Pdgfra+) indicating maturation in the overall OLC population leading up to peak of myelination. While both populations were decreasing in number over time, the ratio of OLs to OPCs remained stable in $\Delta 10/\Delta 10$ s suggesting that the remaining population did not undergo aggregate maturation like the other genotypes (Fig. 6D). Finally, the scale and direction of changes in the number of YFP+ co-expressors were similar to those of their respective single-positive populations (Fig. 6E–G). Taken together, $\Delta 10/\Delta 10$ s demonstrated a significant difference in their ability to produce a large number of OPCs and OLs in the second postnatal week and failed to accumulate adequate numbers of myelinating OLCs.

Defective proliferation and maturation drive oligodendrocyte population dynamics in $\Delta 10$ homozygotes

Given that the overall YFP+ population in $\Delta 10/\Delta 10$ s was already ~50% smaller than that of $+/ \Delta 10$ s at P9, we hypothesized that the

reduced OLC numbers were the result of decreased OPC proliferation, which is typically maximal during the first postnatal week.^{56–58} EdU injections at P9 using a 6-hour exposure protocol to assess the percentage of dividing cells demonstrated decreased EdU+ labelling in $\Delta 10/\Delta 10$ s compared to $+/ \Delta 10$ s, as well as a decrease in the ratio of YFP+EdU+ to total YFP+ cell population. These studies indicated that the loss of proliferative potential occurred both in terms of the absolute number of dividing cells and the relative proportion of dividing cells among the YFP+ population (Fig. 6H–J). These studies explained the altered OLC population dynamics in $\Delta 10/\Delta 10$ s and confirmed that defective proliferation among OPCs immediately precedes hypomyelination in the model.

Since our lineage tracing studies indicated early proliferation deficits in the OPC population, and because the YFP+ population failed to undergo aggregate maturation, we were also interested in the fate of OLCs in $\Delta 10/\Delta 10$ s. Indeed, at P18 we did observe relative increases in the proportion of YFP+Pdgfra+ and YFP+Ng2+ precursors to the total YFP+ population, as well as a relative decrease in the proportion of YFP+CC1+ mature cells to the total YFP+ population in $\Delta 10/\Delta 10$ s (Fig. 6K–M). Therefore, we considered whether stalled proliferation and maturation in OPCs led to apoptosis in a specific subpopulation of YFP+ cells. We stained P9, P14 and P18 sections for Cleaved Caspase 3, a marker of apoptosis.^{25,59} These studies demonstrated little Caspase 3 activation in all brain sections examined, suggesting that apoptosis is not the main cause of the reduced number of OLCs (Supplementary Fig. 8A and B). Representative images of a $+/ \Delta 10$ and $\Delta 10/\Delta 10$ are illustrative of the difference in YFP+ cell numbers at P18 (Fig. 7A and B), suggesting another mechanism of cell loss is at play.

Taken together, we observed specific OLC population dynamics in $\Delta 10/\Delta 10$ s that allowed us to pinpoint both the stage and timing of the defect underlying hypomyelination in the model. Early OPC proliferation was limited, reducing the number of cells with myelinating potential. Fewer OPCs matured and became myelinating cells, resulting in an increased proportion of immature OLCs in $\Delta 10/\Delta 10$ s. Finally, OLCs were progressively lost from the parenchyma, due to an unidentified mechanism. The increased proportion of Pdgfra+ and/or Ng2+ OLCs among remaining YFP+ cells at P18 suggest that these OLCs did not regularly progress past the precursor stage, or that the YFP+ cells that did progress past this stage were less fit. In summary, an early defect in proliferation and subsequent maturation among OPCs leads to reduced numbers of myelinating cells and causes hypomyelination in the $\Delta 10$ model of POLR3B-HLD.

Discussion

Pol III assembly and nuclear import is a complex process, which is known to be perturbed in POLR3-HLD, including in association with mutations in POLR3B.¹⁷ Yee et al.²⁴ assayed the transcriptional function of the mutant complex in zebrafish expressing the Slj mutation constitutively, demonstrating that transcription of pre-tRNA and 7sl Pol III targets were reduced by more than 50% in mutant larvae, while 5Ss levels remained relatively stable. They indirectly demonstrated that Slj impacted Rpc2–Rpc11 (Polr3b–Polr3k) interactions, proposing that the mutation affected Pol III facilitated recycling activity by reducing re-initiation, but did not publish experimental confirmation of the mechanism. Our *in silico* modelling of $\Delta 10$ on the human Pol III structure also indicated the likely interaction of POLR3B exon 10 with POLR3K in the jaw region of the human polymerase. Our proteomics data suggested that POLR3B $\Delta 10$ caused a severe Pol III complex assembly defect, as well as reduced

Figure 3 (Continued)
mice carrying a Pdgfra-CreERT allele and homozygous Polr3b^{fl} alleles; $+/ \Delta 10$ = tamoxifen-treated transgenic mice carrying a Pdgfra-CreERT allele and heterozygous Polr3b^{fl} alleles; CTRL = tamoxifen-treated transgenic mice carrying no Pdgfra-CreERT allele(s); Mbp = myelin basic protein; Olig2 = oligodendrocyte transcription factor 2.

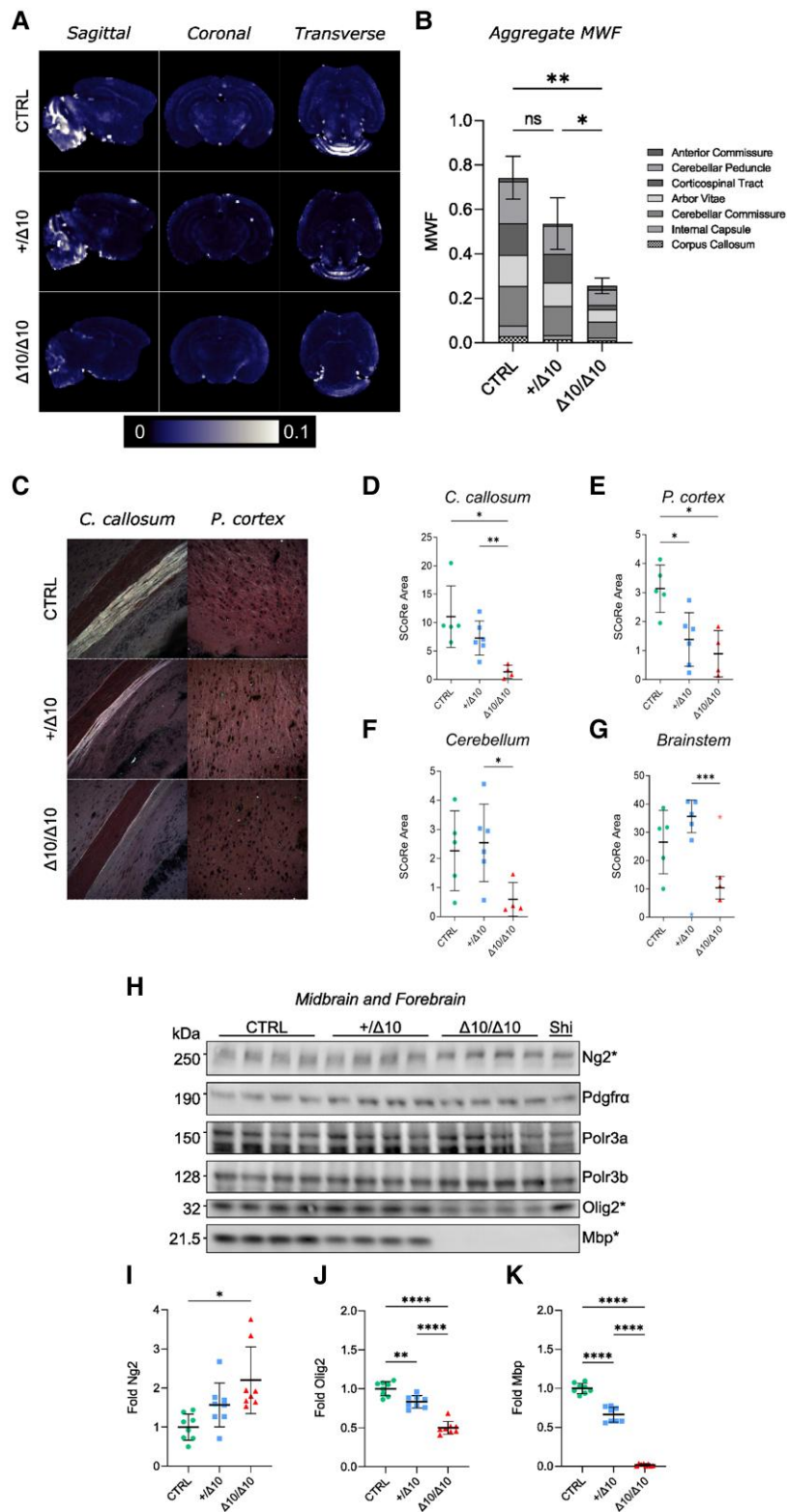


Figure 4 Quantifying hypomyelination in $\Delta 10$ homozygous mice. Hypomyelination was quantified using *ex vivo* MRI (A and B), spectral confocal reflectance (SCoRe) microscopy (C–G), and western blot at peak myelination in mice (H–K). (A) Myelin water fraction (MWF) maps from $\Delta 10/\Delta 10$, $+\Delta 10$ and CTRL mice in sagittal, coronal and transverse views. (B) Summed aggregate MWF values from each region of interest (ROI) in $\Delta 10/\Delta 10$, $+\Delta 10$ and CTRL mice (anterior commissure, cerebellar peduncle, corticospinal tract, arbor vitae, cerebellar commissure, internal capsule, corpus callosum). Error bars reflect standard deviation (SD). Statistical comparison of the $\Delta 10/\Delta 10$ and $+\Delta 10$ was evaluated in the context of a Brown-Forsythe and Welch one-way ANOVA including $\Delta 10/\Delta 10$, $+\Delta 10$, CTRL and tamoxifen-naïve mice. Details can be found in the [Supplementary material](#). (C) Spectral confocal reflectance (SCoRe) microscopy was used to assess label-free sections from $\Delta 10/\Delta 10$ ($n = 4$), $+\Delta 10$ ($n = 6$) and CTRL ($n = 5$) littermates for myelin content at P18. Representative images of the corpus callosum and superficial prefrontal cortex are shown. We quantified myelination as

(continued)

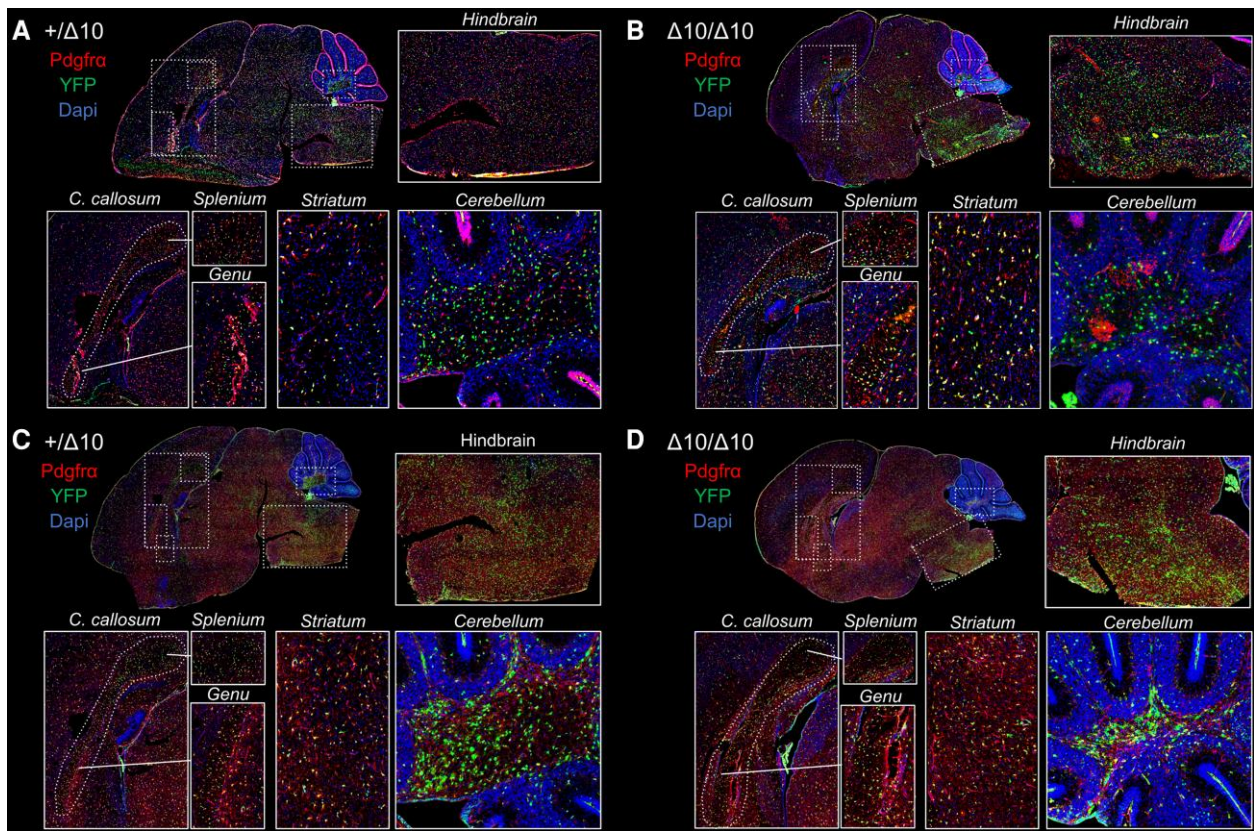


Figure 5 Oligodendrocyte subpopulations appear stable at P9 in $\Delta 10$ homozygous mice. We probed for *Pdgfra* (A and B) and *Ng2* (C and D) protein expression in YFP+ cells at P9 in $+\Delta 10$ s (A and C) and $\Delta 10/\Delta 10$ s (B and D). Cells co-expressing YFP and *Pdgfra* or *Ng2* appeared to be slightly more numerous in $\Delta 10$ heterozygotes relative to homozygotes. Inset pictures display hindbrain (pontomedullary), corpus callosum (splenium and genu), striatum and cerebellar arbor vitae. $\Delta 10/\Delta 10$ = tamoxifen-treated transgenic mice carrying a *Pdgfra-CreERT* allele and homozygous *Polr3b^{fl}* alleles; $+\Delta 10$ = tamoxifen-treated transgenic mice carrying a *Pdgfra-CreERT* allele and heterozygous *Polr3b^{fl}* alleles; CTRL = tamoxifen-treated transgenic mice carrying no *Pdgfra-CreERT* allele(s); C. callosum = corpus callosum; YFP = yellow fluorescent protein; *Pdgfra* = platelet-derived growth factor receptor alpha.

expression of the mutant protein in the cytoplasm and nucleus of human cells.

Based on our proteomics data, we concluded that the main mechanism of Pol III hypofunction resulting from $\Delta 10$ expression is a likely Pol III complex assembly defect, although we could not categorically rule out complex instability. Indeed, we directly demonstrated that $\Delta 10$ has reduced association with Pol III subunits as compared to wild-type protein by AP-MS. However, we also observed that mutant protein was less highly expressed than wild-type at the cytoplasmic and nuclear level when expressed transiently under identical conditions in HEK293T cells. Because Pol III is

assembled in the cytoplasm and then imported into the nucleus,⁶⁰ testing for nuclear expression indirectly supported that $\Delta 10$ does not cause total failure of Pol III complex assembly, consistent with its prior characterization as a hypomorph.^{24,25} Taken together, we confirmed that $\Delta 10$ perturbs the structural integrity of Pol III.

Based on several of our findings, we hypothesize that reduced expression of $\Delta 10$ is related to a process downstream of Pol III complex assembly. Although transcript instability is possible, because we detected similar expression of the orthologous $\Delta 10$ and wild-type mRNA up to 30 days after induction with tamoxifen when validating brain recombination in mouse studies, it is unlikely to be a

Figure 4 (Continued)

S-CoRe area and compared $\Delta 10/\Delta 10$ to $+\Delta 10$ in (D) corpus callosum [−81.2%; Dunnett’s T3: $\mu_{\Delta 10}$ = 1.374; μ_{htz} = 7.304; t = 4.388; df = 6.843; μ_A = 5.930; 95% confidence interval (CI₉₅): 1.801–10.06; P = 0.0089], (E) cortex (−35.6%; Dunnett’s T3: $\mu_{\Delta 10}$ = 0.8910; μ_{htz} = 1.383; t = 0.8958; df = 7.269; μ_A = 0.4920; CI₉₅: −1.186–2.170; P = 0.7562), (F) cerebellum (−76.5%; Dunnett’s T3: $\mu_{\Delta 10}$ = 0.5988; μ_{htz} = 1.945; t = 3.157; df = 7.267; μ_A = 1.945; CI₉₅: 0.06251–3.827; P = 0.0435) and (G) brainstem (−70.8%; Dunnett’s T3: $\mu_{\Delta 10}$ = 10.41; μ_{htz} = 35.65; t = 7.288; df = 5.659; μ_A = 25.24; CI₉₅: 14.19–36.30; P = 0.0009). Mean and standard error are shown. (H) Representative western blots from 15 μg brain lysate samples prepared at P21 where the medulla, pons and cerebellum were removed during dissection. There were no significant differences in *Pdgfra*, *Polr3a* or *Polr3b* protein expression between genotypes. (I) *Ng2* expression tended to be higher in $\Delta 10/\Delta 10$ s than CTRLs but was not differentiated from $+\Delta 10$ s. When comparing $\Delta 10/\Delta 10$ s to $+\Delta 10$ s, (J) *Olig2* was reduced by 40.2% (Dunnett’s T3: $\mu_{\Delta 10}$ = 0.4990; μ_{htz} = 0.8338; t = 8.217; df = 14.00; μ_A = 0.3348; CI₉₅: 0.2252–0.4445; P < 0.0001) and (K) *Mbp* was reduced by 97.3% (Dunnett’s T3: $\mu_{\Delta 10}$ = 0.01785; μ_{htz} = 0.6634; t = 18.83; df = 7.313; μ_A = 0.6455; CI₉₅: 0.5408–0.7502; P < 0.0001). Four male and four female mice (n = 8) of each group listed were used in all western blot studies. Mean and standard deviation are indicated. Except for the MRI quantification detailed above, all statistics were computed using Brown-Forsythe and Welch’s one-way ANOVA with multiple comparisons tested using Dunnett’s T3 method and α = 0.05. * P < 0.05, ** P < 0.01, *** P < 0.001, **** P < 0.0001. $\Delta 10/\Delta 10$ = tamoxifen-treated transgenic mice carrying a *Pdgfra-CreERT* allele and homozygous *Polr3b^{fl}* alleles; $+\Delta 10$ = tamoxifen-treated transgenic mice carrying a *Pdgfra-CreERT* allele and heterozygous *Polr3b^{fl}* alleles; CTRL = tamoxifen-treated transgenic mice carrying no *Pdgfra-CreERT* allele(s); Shi = Shiverer; C. callosum = corpus callosum; P. cortex = prefrontal cortex; *Ng2* = Neuron-gial antigen 2 (encoded by *Cspg4*); *Pdgfra* = Platelet-derived growth factor receptor alpha.

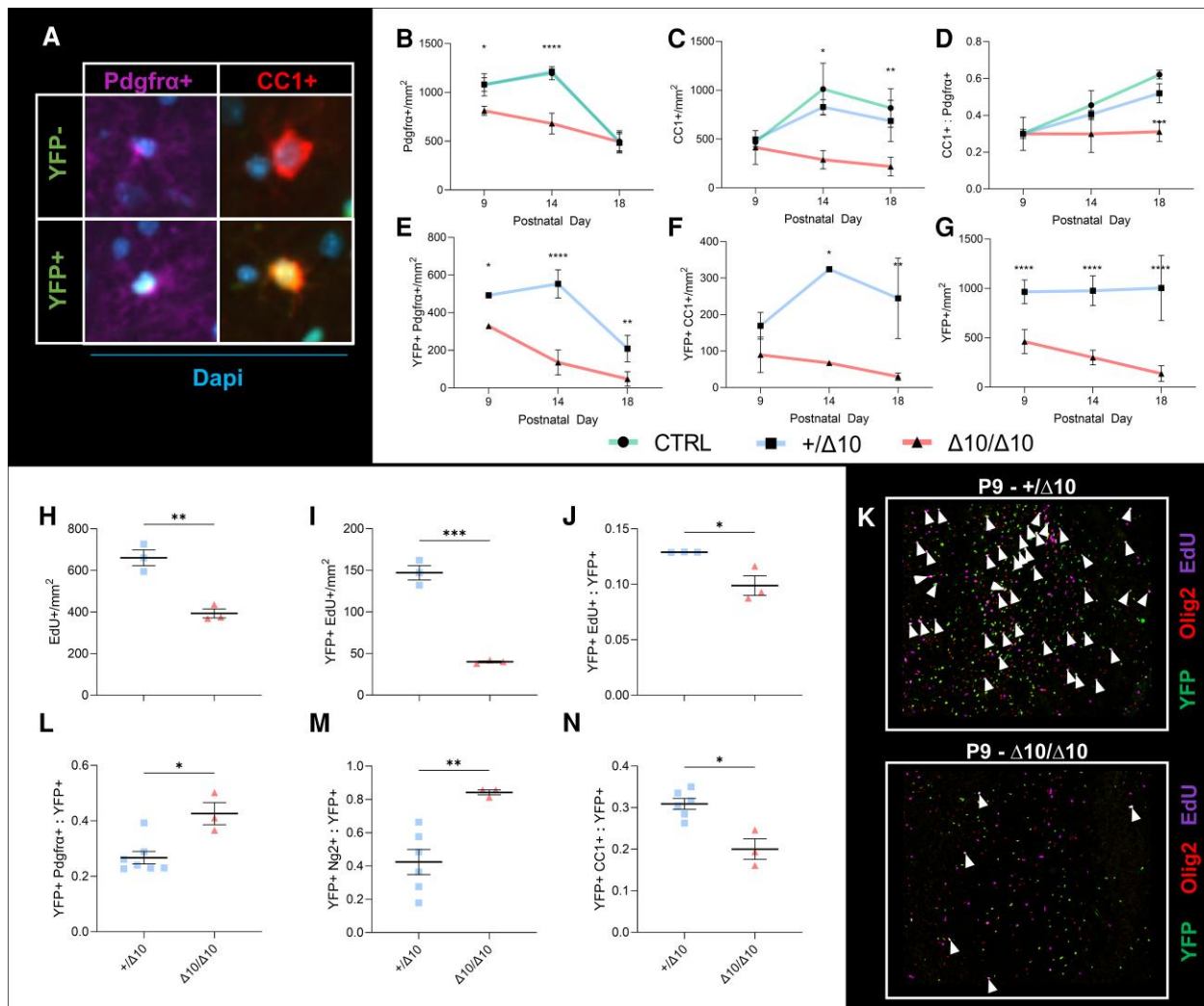


Figure 6 In $\Delta 10$ homozygous mice, hypomyelination is caused by decreased numbers of myelinating oligodendrocytes due to proliferation and maturation defects. (A) Counting yellow fluorescent protein (YFP) positive or negative $Pdgfra+$ OPCs and $CC1+$ mature oligodendrocytes (OLs) in sagittal sections from $\Delta 10/\Delta 10$ s, $+/\Delta 10$ s, and CTRLs allowed us to track the maturation of the oligodendrocyte lineage in transgenic mice. At P9, P14 and P18, counting single-positive (B) $Pdgfra$ precursor or (C) $CC1$ mature oligodendrocyte lineage cells (OLCs) reveals that while CTRLs (green lines) and $+/\Delta 10$ s (blue lines) have similar population dynamics, $\Delta 10/\Delta 10$ s (red lines) fail to increase numbers of precursor and mature OLCs throughout the brain. (D) The maturation of the overall population is demonstrated as an increasing ratio of $CC1+$ mature OLCs to $Pdgfra+$ precursors in CTRL and $+/\Delta 10$ mice, but this does not occur in $\Delta 10/\Delta 10$ s. (E) $YFP+Pdgfra+$ OPC dynamics largely mirror the scale and direction of changes in the single positive $Pdgfra$ population. (F) $YFP+CC1+$ OLC dynamics largely mirror the scale and direction of changes in the single positive $CC1$ population. (G) $YFP+$ cell numbers decline throughout the observation window, suggesting that while adequate numbers of OLCs are not produced in $\Delta 10/\Delta 10$ s, existing cells are also depleted from the parenchyma over time. Mean of biological replicates and standard deviations are shown for the plots in B–G, animal numbers and biological replicates for each time series are detailed in [Supplementary Table 3](#). Statistics for graphs in B–G were computed using two-way ANOVA with multiple comparisons (between genotypes at each time point) tested using the Tukey method and $\alpha = 0.05$. (H–J) Proliferation at P9 as assessed by EdU incorporation after a 6 h labelling protocol is reduced in $\Delta 10/\Delta 10$ s compared to $+/\Delta 10$ s in terms of (H) number of proliferating cells, (I) number of $YFP+$ proliferating cells, and (J) the relative proportion of proliferating cells among $YFP+$ cells. (L–N) At P18, a higher proportion of OLCs in $\Delta 10/\Delta 10$ s are immature compared to $+/\Delta 10$ s. (L) A higher proportion of $YFP+$ cells co-express $Pdgfra$. (M) A higher proportion of $YFP+$ cells co-express $Ng2$. (N) At P18, $\Delta 10/\Delta 10$ s have a lower proportion of mature OLCs compared to $+/\Delta 10$ s. A lower proportion of $YFP+$ cells co-express $CC1$. (K) Cells triple labelled for YFP, Olig2 and EdU (white arrowheads) are significantly more numerous in $+/\Delta 10$ s (upper panel) than in $\Delta 10/\Delta 10$ s (lower panel). Statistics for graphs in H–N were computed using unpaired, two-tailed t-tests with Welch’s correction and $\alpha = 0.05$. * $P < 0.05$, ** $P < 0.01$, *** $P < 0.001$, **** $P < 0.0001$. $\Delta 10/\Delta 10$ = tamoxifen-treated transgenic mice carrying a $Pdgfra-CreERT$ allele and homozygous $Polr3b^fl$ alleles; $+/\Delta 10$ = tamoxifen-treated transgenic mice carrying a $Pdgfra-CreERT$ allele and heterozygous $Polr3b^fl$ alleles; CTRL = tamoxifen-treated transgenic mice carrying no $Pdgfra-CreERT$ allele(s); SEM = standard error of the mean; $Pdgfra$ = platelet-derived growth factor receptor alpha; $CC1$ = clone CC1 of anti-adenomatous polyposis coli (also: Anti-Quaking 7); $Ng2$ = Neuron-glia antigen 2 (encoded by *Cspg4*); EdU = 5-ethynyl-2'-deoxyuridine.

significant factor *in vivo*. Moreover, we did not detect multiple splice products in transgenic mice, suggesting that the mutant exon 9–11 junction is a stable product, and that nonsense-mediated decay is unlikely. Finally, *in silico* analysis does not suggest that free (unassembled) human $\Delta 10$ has reduced half-life compared to its

wild-type protein counterpart.⁶¹ In summary, evidence of transcript instability was not observed *in vivo* using a highly similar orthologous mutant, while the free mutant protein is not expected to have reduced half-life. We therefore propose that reduced expression of the mutant detected in our human *in vitro* assays is

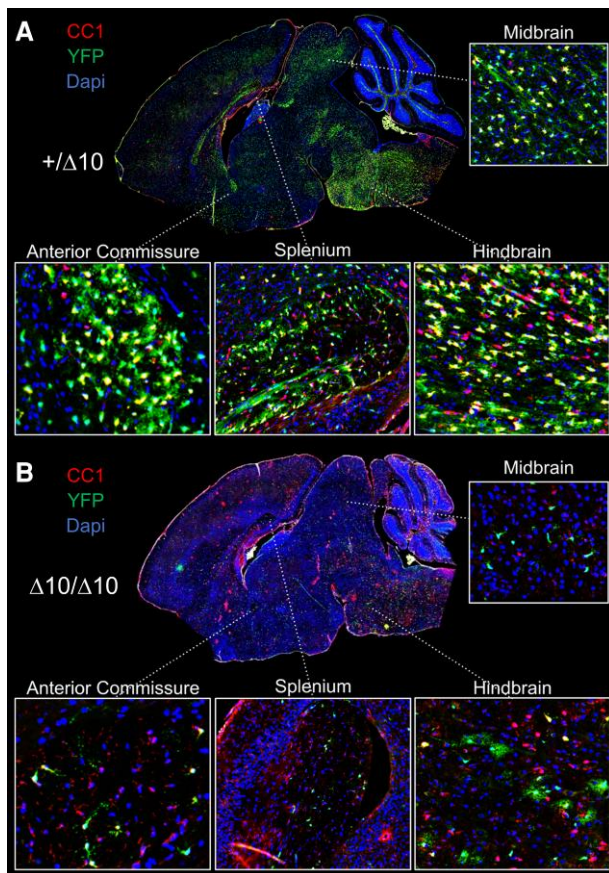


Figure 7 Depletion of YFP+ cells from the parenchyma in $\Delta 10$ homozygous mice. Comparison of $+\Delta 10$ (A) and $\Delta 10/\Delta 10$ (B) demonstrated widespread depletion of yellow fluorescent protein positive (YFP+) cells in the parenchyma of $\Delta 10/\Delta 10$. Representative images shown. Among remaining YFP+ cells, $\Delta 10/\Delta 10$ had cells with shorter processes and more immature morphology. Inset pictures show the hindbrain, midbrain, splenium of the corpus callosum, and anterior commissure. $\Delta 10/\Delta 10$ = tamoxifen-treated transgenic mice carrying a *Pdgfra-CreERT* allele and homozygous *Polr3b^f* alleles; $+\Delta 10$ = tamoxifen-treated transgenic mice carrying a *Pdgfra-CreERT* allele and heterozygous *Polr3b^f* alleles; CTRL = tamoxifen-treated transgenic mice carrying no *Pdgfra-CreERT* allele(s); CC1 = clone CC1 of anti-adenomatous polyposis coli (also: Anti-Quaking 7).

due to turnover of subunits that fail to be assembled into functional enzymes. In summary, we have elucidated that $\Delta 10$ impairs Pol III complex assembly or stability, thereby disrupting its physiological functions upstream of transcription. On the basis of these findings, we elected to study $\Delta 10$ in the context of oligodendrocyte development and myelination.

The mutation employed in our study explores an alternative molecular mechanism in line with prior characterization of disease-causing variants including a POLR3B variant that causes POLR3-HLD and impairs Pol III assembly or stability.^{3,17} Indeed, recent attempts to recapitulate POLR3-HLD *in vivo* have largely been unsuccessful with the exception of a recent study by Merheb *et al.*,¹⁸ where a constitutively lethal W671R/G672E double mutation in *Polr3a* was used in the context of a Cre/Lox strategy to elicit a myelin phenotype. The orthologous mutation used in Merheb *et al.*¹⁸ has ~30% of the transcriptional activity of WT Pol III in *Saccharomyces cerevisiae*, but complex assembly was not assayed directly. Complex assembly is not known to be significantly affected in the single G672E mutant,¹⁶ and the orthologous

Y685K/G686E yeast mutant described in Moir *et al.*¹⁹ is not expected to affect subunit interactions. Taken together, there are now two mechanistic models of POLR3-HLD: a milder neurological phenotype based on a *Polr3a* double mutant that causes reduced Pol III transcriptional output,¹⁸ and our more severe model based on a *Polr3b* mutation that perturbs Pol III structural integrity.

We chose to use an inducible/conditional strategy to direct expression of $\Delta 10$ to OPCs using a *Pdgfra-CreERT*-driven approach because it allowed us to study postnatal development, a critical period of myelinogenesis in the brain. Using an inducible/conditional approach to study myelination has several advantages, the most significant being that lethality is avoidable and the severity of the phenotype can be titrated. Because we elected to study the early oligodendrocyte lineage and OPCs are generated throughout development, we were faced with the reality that we would not be able to induce complete tissue recombination.^{62,63} Because of this, we elected to use a triple transgenic strategy in order to better understand the contributions of recombined and non-recombined cells to the overall CNS pathology. Using this method, we observed significant hypomyelination associated with YFP+ cell dysfunction, namely proliferation and maturation defects, despite the presence of YFP-, non-recombined cells. The reporter used in the study is known to be highly specific to recombined cells but is less sensitive and may underestimate the true recombination rate.⁶⁴ This is consistent with our finding that CC1+ cell density decreased in $\Delta 10/\Delta 10$ mice to a slightly greater degree than would be explained by the decrease in YFP+CC1+ cells alone (compare Fig. 6C with Fig. 6F). Therefore, it is likely that the observed pathology was less affected by non-recombined cells than would be anticipated based on our YFP-based estimate of recombination rate. Altogether, we did not observe evidence that non-recombined cells had a material impact on our experimental outcomes, which showed remarkable correlation to key aspects of the human disease.

Recombination rates were not amenable to augmentation by administering tamoxifen earlier, or for longer periods. In early pilot studies we found that prenatal tamoxifen administration caused difficulties during parturition in line with prior studies.⁶⁵ Furthermore, the doses of tamoxifen used in our study were at the upper limit of tolerability, precluding extended treatment in the context of a comparable dosing regimen. Finally, we observed reduced myelination in CTRL mice at tolerable doses as compared to tamoxifen-naïve mice, in contrast to *in vitro* and *in vivo* studies suggesting that tamoxifen increases remyelination in mice (Supplementary Fig. 4).^{66,67} This conflict in experimental observations may be due to either pharmacokinetic differences between the studies (dosing, neonatal versus adult pharmacokinetic differences), or differences in tamoxifen pharmacodynamics in the context of myelination versus remyelination. Our pilot studies that identified an effect of tamoxifen on myelination led us to design our experiments with equal tamoxifen exposure in all comparator groups.

Emergence of non-CNS anomalies such as hypodontia and craniofacial abnormalities are expected to be caused by *Pdgfra* expression in non-CNS tissues. Indeed, although *Pdgfra* is a high-fidelity marker of the early oligodendrocyte lineage in the mouse CNS, it is widely expressed along the developmental continuum in various neural crest derivatives throughout the body including the developing craniofacial bones and teeth.^{68–70} We observed an absence of incisors in approximately half of $\Delta 10/\Delta 10$ s and small incisors among the rest. Given that many $\Delta 10/\Delta 10$ s did not have eruption prior to death, we assume that eruption is not merely delayed but rather that incisors are significantly underdeveloped, most likely

due to an underlying hypoplasia. The manifestation of hypomyelination, hypodontia and craniofacial abnormalities is interesting and suggests that further study of the functional similarities between neural crest-derived mesenchymal derivatives and oligodendrocytes may yield greater understanding of the mechanistic link between the disparate phenotypes observed in POLR3-HLD.

Altogether, we conducted an array of studies to confirm and determine the extent of hypomyelination in our transgenic mice. Several histological and biochemical measurements we performed suggested that $+\Delta 10$ s were not physiologically equivalent to CTRLs. POLR3-HLD is recessive, and heterozygotes/carriers are not known to have hypomyelination or associated clinical deficits. We attributed differences in results between CTRLs and $+\Delta 10$ s to the increased sensitivity afforded by studying the $\Delta 10$ mutation at different allelic doses on a genetically identical background. Moreover, the histological and biochemical studies performed here are also incredibly sensitive to changes in myelination relative to clinical MRI used in patient studies. Importantly, we did not observe behavioural or other obvious phenotypic differences between $+\Delta 10$ s and CTRLs. Therefore, we determined that characterizing the phenotype in $\Delta 10/\Delta 10$ s by comparing to $+\Delta 10$ s was most apt, given that the only genetic difference between the two groups is the additional $\Delta 10$ allele. Unfortunately, we could not compare our findings in $+\Delta 10$ mice to the prior published *Polr3a* model, because Merheb et al.¹⁸ limited their study to comparisons with wild-type mice. We found that $+\Delta 10$ and CTRL mice have minor differences in oligodendrocyte physiology based on tissue-level measurements. Their similarity in terms of the observed myelination outcomes emphasizes that not all cell-level changes will cause defective myelination outcomes *in vivo* due to reserve capacity in the myelinating population. Moreover, this highlights the importance of *in vivo* studies for evaluating whether a particular mutation will produce hypomyelination.

Studies of myelination confirmed severe hypomyelination in $\Delta 10/\Delta 10$ s. Notably, marked decreases in Mbp immunofluorescence were identified in sagittal and hemi-coronal sections (Supplementary Fig. 3). Hemi-coronal sections demonstrated a certain degree of spatial variability in the Mbp signal, which may reflect the contribution of cells that did not undergo cre-mediated recombination during tamoxifen exposure. However, we noted that the pattern of preserved myelination corresponded to spinal cord, subcortical areas corresponding to the posterior internal capsule and pallidum, and corpus callosum. Patients with POLR3-HLD are known to have preserved myelination in specific structures, including in the pallidum and corticospinal tracts at the level of the posterior limb of the internal capsule. Therefore, this variability may also be reflective of intrinsic differences in the response of these brain areas to Pol III hypofunction in mice, similar to the human disease. *Ex vivo* MRI and other histological studies (e.g., SCoRe imaging) focusing on quantification of myelin lipids agreed with the immunofluorescence results. Depending on the modality of inquiry and brain region, we detected anywhere from ~50% to >80% loss of myelin at P18.

Histological results were validated by western blot using mid-brain/forebrain tissue lysates at the peak of myelination (P21). Midbrain and forebrain Mbp expression was reduced by >97%, but the exact percentage cannot be ascertained due to a floor effect. Our panel of immunoblotting antibodies also revealed reduced Olig2 expression, which likely reflects reduced numbers of OLCs. Among the other targets tested, none suggested significant changes at the tissue level. As expected, we did not detect significantly reduced *Polr3b* expression in our *in vivo* western blots due to using

samples in which mutant cells make up a small percentage of the dissected tissue. *Ex vivo* MRI and histological studies agreed with our studies of OLC protein expression, however our western blot data suggested a more severe decrease in Mbp as compared to the imaging studies focusing on regions of interest that are heavily myelinated. While it is expected to see more severe decreases on western blot since aggregate Mbp across both grey and white matter regions is measured, it is possible that myelin components may be lost to a more severe degree than the cells themselves due to dysfunction among remaining OLCs. In a recent study published by our lab, we observed that *Polr3b* knockdown was associated with reduced expression of markers of myelination in differentiating oligodendrocytes, including substantially reduced Mbp transcription.⁷¹ Because we also observed evidence of differentiation defects, it is likely that remaining CC1+ cells are dysfunctional, explaining the discrepancy in the scale of decreases in Mbp expression and loss of CC1+ cells. Taken together, the model recapitulated severe hypomyelination and produced effect sizes that will be useful for testing therapeutic interventions in the future.

Using lineage tracing methods, we tracked the fate of subpopulations of oligodendrocytes to ascertain the mechanism of hypomyelination. From the outset, we were specifically interested in the question of whether hypomyelination in POLR3-HLD is caused by a failure to obtain adequate numbers of myelinating cells or defective cell function leading to improper or reduced production of myelin and/or myelin components such as Mbp. Our finding that YFP+ cell numbers were already reduced by 50% relative to heterozygotes at P9 suggested a proliferation defect that preceded our observation window, consistent with maximal CNS *Pdgfra*+ cell proliferation from late gestation through the first postnatal week.^{56–58} Indeed, we observed that the $\Delta 10/\Delta 10$ OPC population did not undergo a rapid increase in size from P9 to P14, and mature OLCs did not accumulate in the brain from P9 onward. Direct testing of proliferation with EdU labelling confirmed this hypothesis and demonstrated that a significant proliferation defect was the most upstream factor leading to hypomyelination in our model. Because we did not detect activated Caspase 3 at P9 (or afterward), we concluded that the abrogated proliferation and maturation of the OLC lineage in the early stages produced inadequate numbers of myelinating cells and was directly responsible for the observed hypomyelination.

Our model differs from that described by Merheb et al.¹⁸ in that we developed it based on mutation of *Polr3b*, and moreover using a mutation that causes defective Pol III biogenesis. Indeed, our model is more severe and uniquely produces CNS-dependent phenotypes common among hypo/dysmyelination mouse models, including ataxia, tremor, seizures and early death.^{72–76} We expect this to be the case because Pol III complex assembly is upstream from transcription, and disruption of upstream processes typically lead to more wide-ranging effects on cell physiology. Moreover, we detected and quantified a specific defect in proliferation, which occurred at a critical developmental time point, immediately prior to the peak of myelination. This is likely to play a major role in the development of hypomyelination in our model and is also expected to be an underlying factor in the difference in severity between our observations and those of Merheb et al.¹⁸

We detected steadily decreasing numbers of YFP+ cells in homozygous mice across all endpoints, which decreased in number throughout the observation window. The dwindling numbers of OLCs demonstrated in our model were also suggested by the findings of Merheb et al.¹⁸ Therefore, two animal models making use

of mutations in distinct genes, causing Pol III dysfunction by different mechanisms, suggest that reduced myelinogenesis is related to reduced numbers of myelinating cells. Although we cannot yet say with certainty that this is true in POLR3-HLD, in the only existing study quantifying oligodendrocyte-specific immunohistochemistry in a patient, OLIG2+ cells were reduced in number by 70–99% when compared to a control, depending on the brain region.¹¹ Therefore, our current understanding of POLR3-HLD pathophysiology indicates that putative interventions should be targeted to early stages of the oligodendrocyte lineage in order to produce therapeutic benefit, in line with recently published hypotheses by Perrier and colleagues.⁷⁷

Conclusions

In this study, we characterized the POLR3BA10 mutation in human cells and developed an animal model of POLR3-HLD using the orthologous mutation in mice. Our proteomics studies demonstrated that $\Delta 10$ impacts Pol III structural integrity, likely by impairing assembly of the complex. Postnatal expression of the $\Delta 10$ mutant early in the oligodendrocyte lineage using an inducible/conditional strategy in mice recapitulated recessive disease features such as hypomyelination, hypodontia and craniofacial abnormalities. In the CNS, homozygous $\Delta 10$ expression was associated with severe hypomyelination, which was caused by significant proliferation and maturation defects in OPCs. Taken together, we produced a unique and novel model of POLR3-HLD: the first of its kind to be based on *Polr3b* mutation and to recapitulate patients' neurological and craniofacial/dental abnormalities, opening the door to further study disease mechanisms and test potential therapeutics.

Data availability

Original data underlying this manuscript that were generated at MyeliNeuroGene lab can be obtained from the corresponding author on reasonable request. Of note, a substantial portion of the original data are available as [Supplementary material](#). Original craniofacial data generated at the University of Missouri, Kansas City, and the Stowers Institute for Medical Research, can be accessed from the Stowers Institute Original Data Repository at <http://www.stowers.org/research/publications/lipbp-2400>.

Acknowledgements

The authors would like to acknowledge Dr. Klaus Kaestner and Dr. Michael Pack (University of Pennsylvania), Dr. William Richardson (University College London), Dr. Brian Popko (Northwestern University) and Mitra Cowan (McGill Integrated Core for Animal Modelling) for contributing mouse strains and/or technical expertise to the development of the *Polr3b* $\Delta 10$ mouse model.

Funding

This research was funded by research grants from the Yaya Foundation for 4H leukodystrophy, the Montreal Children's Hospital Foundation (Tallman Family), and Leuco Action. G.B. has received a Clinical Research Scholar Junior 1 award from the Fonds de Recherche du Quebec – Santé (FRQS) (2012–2016), New Investigator Salary Award from the Canadian Institutes of Health Research (2017–2022) and Senior Clinical Research Scholar award from the FRQS (2022–2025). D.C. is supported by an MS Society of Canada graduate studentship award. N.A.U. holds a post-doctoral

fellowship funded by Hoffmann-La Roche Limited. M.A.M.-R. is supported by a Vanier Canada Graduate Scholarship and the McGill Faculty of Medicine and Health Sciences. T.C.C. is supported by a Stowers Family Endowment for Dental and Mineralized Tissue Research. K.E.N.W. is funded by a Transition to Independence Award from the National Institute of Dental and Craniofacial Research (K99DE030971). P.A.T. is supported by the Stowers Institute for Medical Research (1008).

Competing interests

G.B. was a consultant for Passage Bio Inc (2020–2022) and Ionis (2019). She is/was a site investigator for the Alexander's disease trial of Ionis (2021–present), Metachromatic leukodystrophy of Shire/Takeda (2020–2021), Krabbe and GM1 gene therapy trials of Passage Bio (2021–present), GM1 natural history study from the University of Pennsylvania sponsored by Passage Bio (2021–present) and Adrenoleukodystrophy/Hematopoietic stem cell transplantation natural history study of Bluebird Bio (2019), a site sub-investigator for the MPS II gene therapy trial of Regenxbio (2021–present) and the MPS II clinical trial of Denali (2022–present). She has received unrestricted educational grants from Takeda (2021–2022). The other authors have no competing interests.

Supplementary material

[Supplementary material](#) is available at *Brain* online.

References

- Bernard G, Chouery E, Putorti ML, et al. Mutations of POLR3A encoding a catalytic subunit of RNA polymerase pol III cause a recessive hypomyelinating leukodystrophy. *Am J Hum Genet.* 2011; 89:415–423.
- Tetreault M, Choquet K, Orcesi S, et al. Recessive mutations in POLR3B, encoding the second largest subunit of pol III, cause a rare hypomyelinating leukodystrophy. *Am J Hum Genet.* 2011; 89:652–655.
- Thiffault I, Wolf NI, Forget D, et al. Recessive mutations in POLR1C cause a leukodystrophy by impairing biogenesis of RNA polymerase III. *Nat Commun.* 2015;6:7623–7631.
- Dorboz I, Dumay-Odelot H, Boussaid K, et al. Mutation in POLR3K causes hypomyelinating leukodystrophy and abnormal ribosomal RNA regulation. *Neurol Genet.* 2018;4:e289.
- Saitu H, Osaka H, Sasaki M, et al. Mutations in POLR3A and POLR3B encoding RNA polymerase III subunits cause an autosomal-recessive hypomyelinating leukoencephalopathy. *Am J Hum Genet.* 2011;89:644–651.
- Soderholm HE, Chapin AB, Bayrak-Toydemir P, Bonkowsky JL. Elevated leukodystrophy incidence predicted from genomics databases. *Pediatr Neurol.* 2020;111:66–69.
- Bernard G, Vanderver A. POLR3-related leukodystrophy. In: Adam MP, Mirzaa GM, Pagon RA, et al, eds. *GeneReviews*®. University of Washington; 2012 [Updated 2017].
- Pelletier F, Perrier S, Cayami FK, et al. Endocrine and growth abnormalities in 4H leukodystrophy caused by variants in POLR3A, POLR3B, and POLR1C. *J Clin Endocrinol Metab.* 2021;106:e660–e674.
- Gauquelin L, Cayami FK, Sztriha L, et al. Clinical spectrum of POLR3-related leukodystrophy caused by biallelic POLR1C pathogenic variants. *Neurol Genet.* 2019;5:e369.
- Wolf NI, Vanderver A, van Spaendonk RM, et al. Clinical spectrum of 4H leukodystrophy caused by POLR3A and POLR3B mutations. *Neurology.* 2014;83:1898–1905.

11. Vanderver A, Tonduti D, Bernard G, et al. More than hypomyelination in Pol-III disorder. *J Neuropathol Exp Neurol.* 2013;72:67-75.
12. Steenweg ME, Vanderver A, Blaser S, et al. Magnetic resonance imaging pattern recognition in hypomyelinating disorders. *Brain.* 2010;133:2971-2982.
13. Schiffmann R, van der Knaap MS. Invited article: An MRI-based approach to the diagnosis of white matter disorders. *Neurology.* 2009;72:750-759.
14. La Piana R, Tonduti D, Gordish Dressman H, et al. Brain magnetic resonance imaging (MRI) pattern recognition in Pol III-related leukodystrophies. *J Child Neurol.* 2014;29:214-220.
15. Watt KEN, Macintosh J, Bernard G, Trainor PA. RNA polymerases I and III in development and disease. *Semin Cell Dev Biol.* 2023;136:49-63.
16. Choquet K, Yang S, Moir RD, et al. Absence of neurological abnormalities in mice homozygous for the Polr3a G672E hypomyelinating leukodystrophy mutation. *Mol Brain.* 2017;10:13.
17. Choquet K, Pinaud M, Yang S, et al. The leukodystrophy mutation Polr3b R103H causes homozygote mouse embryonic lethality and impairs RNA polymerase III biogenesis. *Mol Brain.* 2019;12:59.
18. Merheb E, Cui MH, DuBois JC, et al. Defective myelination in an RNA polymerase III mutant leukodystrophic mouse. *Proc Natl Acad Sci U S A.* 2021;118:e2024378118.
19. Moir RD, Lavados C, Lee J, Willis IM. Functional characterization of Polr3a hypomyelinating leukodystrophy mutations in the *S. cerevisiae* homolog, RPC160. *Gene.* 2021;768:145259.
20. Kim H, Kim M, Im SK, Fang S. Mouse Cre-LoxP system: General principles to determine tissue-specific roles of target genes. *Lab Anim Res.* 2018;34:147-159.
21. Betz UA, Vossenrich CA, Rajewsky K, Müller W. Bypass of lethality with mosaic mice generated by Cre-loxP-mediated recombination. *Curr Biol.* 1996;6:1307-1316.
22. Choquet K, Forget D, Meloche E, et al. Leukodystrophy-associated POLR3A mutations down-regulate the RNA polymerase III transcript and important regulatory RNA BC200. *J Biol Chem.* 2019;294:7445-7459.
23. Azmanov DN, Siira SJ, Chamova T, et al. Transcriptome-wide effects of a POLR3A gene mutation in patients with an unusual phenotype of striatal involvement. *Hum Mol Genet.* 2016;25:4302-4314.
24. Yee NS, Gong W, Huang Y, et al. Mutation of RNA Pol III subunit *rpc2/polr3b* leads to deficiency of subunit *Rpc11* and disrupts zebrafish digestive development. *PLoS Biol.* 2007;5:e312.
25. Kieckhaefer J, Lukovac S, Ye DZ, et al. The RNA polymerase III subunit *Polr3b* is required for the maintenance of small intestinal crypts in mice. *Cell Mol Gastroenterol Hepatol.* 2016;2:783-795.
26. Gutierrez M, Thiffault I, Guerrero K, et al. Large exonic deletions in POLR3B gene cause POLR3-related leukodystrophy. *Orphanet J Rare Dis.* 2015;10:69-73.
27. Milovanova N ZEY, Mikhailova SV, Pechatnikova N, Fedonyk I. Two possible new mutations of the POLR3B gene in Russian patients with hypomyelinating leukodystrophies (P-496). *J Inherited Metabolic Dis.* 2014;37:27-185.
28. Daoud H, Tetreault M, Gibson W, et al. Mutations in POLR3A and POLR3B are a major cause of hypomyelinating leukodystrophies with or without dental abnormalities and/or hypogonadotropic hypogonadism. *J Med Genet.* 2013;50:194-197.
29. Kulhánek J, Brožová K, Hansíková H, et al. POLR3B-associated leukodystrophy: Clinical, neuroimaging and molecular-genetic analyses in four patients: Clinical heterogeneity and novel mutations in POLR3B gene. *Neurol Neurochir Pol.* 2019;53:369-376.
30. Montenegro LR, Freitas MR, Trarbach EB, et al. Mutational analysis of POLR3A and POLR3B genes in patients with 4H syndrome and isolated hypogonadotropic hypogonadism: Is there a link between these two conditions? *Endocr Rev.* 2013;34:i397.
31. Vanderver A, Simons C, Helman G, et al. Whole exome sequencing in patients with white matter abnormalities. *Ann Neurol.* 2016;79:1031-1037.
32. Jurkiewicz E, Dunin-Wąsowicz D, Gieruszczak-Białek D, et al. Recessive mutations in POLR3B encoding RNA polymerase III subunit causing diffuse hypomyelination in patients with 4H leukodystrophy with polymicrogyria and cataracts. *Clin Neuroradiol.* 2017;27:213-220.
33. Krygier M, Kwarcianny M, Wasilewska K, et al. A study in a Polish ataxia cohort indicates genetic heterogeneity and points to MTCL1 as a novel candidate gene. *Clin Genet.* 2019;95:415-419.
34. Kean MJ, Couzens AL, Gingras AC. Mass spectrometry approaches to study mammalian kinase and phosphatase associated proteins. *Methods.* 2012;57:400-408.
35. The UniProt Consortium. Uniprot: The universal protein knowledgebase. *Nucleic Acids Res.* 2017;45:D158-D169.
36. The UniProt Consortium. Uniprot: The universal protein knowledgebase. *Nucleic Acids Res.* 2018;46:2699-2699.
37. Tyanova S, Temu T, Sinitcyn P, et al. The Perseus computational platform for comprehensive analysis of (prote)omics data. *Nat Methods.* 2016;13:731-740.
38. Kang SH, Fukaya M, Yang JK, Rothstein JD, Bergles DE. NG2+ CNS glial progenitors remain committed to the oligodendrocyte lineage in postnatal life and following neurodegeneration. *Neuron.* 2010;68:668-681.
39. Srinivas S, Watanabe T, Lin C-S, et al. Cre reporter strains produced by targeted insertion of EYFP and ECFP into the ROSA26 locus. *BMC Dev Biol.* 2001;1:4.
40. Ladner CL, Yang J, Turner RJ, Edwards RA. Visible fluorescent detection of proteins in polyacrylamide gels without staining. *Anal Biochem.* 2004;326:13-20.
41. Lu W, Yu H, Shimakawa A, Alley M, Reeder SB, Hargreaves BA. Water-fat separation with bipolar multiecho sequences. *Magn Reson Med.* 2008;60:198-209.
42. Kellner E, Dhital B, Kiselev VG, Reisert M. Gibbs-ringing artifact removal based on local subvoxel-shifts. *Magn Reson Med.* 2016;76:1574-1581.
43. Lee J, Hyun JW, Lee J, et al. So you want to image myelin using MRI: An overview and practical guide for myelin water imaging. *J Magn Reson Imaging.* 2021;53:360-373.
44. Liu H, Grouza V, Tuznik M, et al. Self-labelled encoder-decoder (SLED) for multi-echo gradient echo-based myelin water imaging. *NeuroImage.* 2022;264:119717.
45. Dorr AE, Lerch JP, Spring S, Kabani N, Henkelman RM. High resolution three-dimensional brain atlas using an average magnetic resonance image of 40 adult C57Bl/6J mice. *Neuroimage.* 2008;42:60-69.
46. Stirling DR, Swain-Bowden MJ, Lucas AM, Carpenter AE, Cimini BA, Goodman A. Cellprofiler 4: Improvements in speed, utility and usability. *BMC Bioinform.* 2021;22:433.
47. Stirling DR, Carpenter AE, Cimini BA. Cellprofiler analyst 3.0: Accessible data exploration and machine learning for image analysis. *Bioinformatics.* 2021;37:3992-3994.
48. McQuin C, Goodman A, Chernyshev V, et al. Cellprofiler 3.0: Next-generation image processing for biology. *PLoS Biol.* 2018;16:e2005970.
49. Dobson ETA, Cimini B, Klemm AH, Wählby C, Carpenter AE, Eliceiri KW. Imagej and CellProfiler: Complements in open-source bioimage analysis. *Curr Protoc.* 2021;1:e89.
50. Dao D, Fraser AN, Hung J, Ljosa V, Singh S, Carpenter AE. Cellprofiler analyst: Interactive data exploration, analysis and

- classification of large biological image sets. *Bioinformatics (Oxford, England)*. 2016;32:3210-3212.
51. Vora SR, Camci ED, Cox TC. Postnatal ontogeny of the cranial base and craniofacial skeleton in male C57BL/6J mice: A reference standard for quantitative analysis. *Front Physiol*. 2015;6:417.
 52. Girbig M, Misiaszek AD, Vorländer MK, et al. Cryo-EM structures of human RNA polymerase III in its unbound and transcribing states. *Nat Struct Mol Biol*. 2021;28:210-219.
 53. Djordjevic D, Pinard M, Gauthier MS, et al. De novo variants in POLR3B cause ataxia, spasticity, and demyelinating neuropathy. *Am J Hum Genet*. 2021;108:186-193.
 54. Schain AJ, Hill RA, Grutzendler J. Label-free in vivo imaging of myelinated axons in health and disease with spectral confocal reflectance microscopy. *Nat Med*. 2014;20:443-449.
 55. Foran DR, Peterson AC. Myelin acquisition in the central nervous system of the mouse revealed by an MBP-Lac Z transgene. *J Neurosci*. 1992;12:4890-4897.
 56. Nishiyama A, Lin X-H, Giese N, Heldin C-H, Stallcup WB. Co-localization of NG2 proteoglycan and PDGF α -receptor on O2A progenitor cells in the developing rat brain. *J Neurosci Res*. 1996;43:299-314.
 57. Nishiyama A, Lin X-H, Giese N, Heldin C-H, Stallcup WB. Interaction between NG2 proteoglycan and PDGF α -receptor on O2A progenitor cells is required for optimal response to PDGF. *J Neurosci Res*. 1996;43:315-330.
 58. Robinson AP, Rodgers JM, Goings GE, Miller SD. Characterization of oligodendroglial populations in mouse demyelinating disease using flow cytometry: Clues for MS pathogenesis. *PLoS One*. 2014;9:e107649.
 59. Porter AG, Jänicke RU. Emerging roles of caspase-3 in apoptosis. *Cell Death Differ*. 1999;6:99-104.
 60. Wild T, Cramer P. Biogenesis of multisubunit RNA polymerases. *Trends Biochem Sci*. 2012;37:99-105.
 61. Gasteiger E, Hoogland C, Gattiker A, et al. Protein identification and analysis tools on the ExpASY server. In: Walker JM, ed. *The proteomics protocols handbook*. Humana Press; 2005:571-607.
 62. Kessar N, Fogarty M, Iannarelli P, Grist M, Wegner M, Richardson W. Competing waves of oligodendrocytes in the forebrain and postnatal elimination of an embryonic lineage. *Nat Neurosci*. 2006;9:173-179.
 63. Richardson WD, Kessar N, Pringle N. Oligodendrocyte wars. *Nat Rev Neurosci*. 2006;7:11-18.
 64. McKenzie IA, Ohayon D, Li H, et al. Motor skill learning requires active central myelination. *Science*. 2014;346:318-322.
 65. Lizen B, Claus M, Jeannotte L, Rijli FM, Gofflot F. Perinatal induction of Cre recombination with tamoxifen. *Transgenic Res*. 2015;24:1065-1077.
 66. Gonzalez GA, Hofer MP, Syed YA, et al. Tamoxifen accelerates the repair of demyelinated lesions in the central nervous system. *Sci Rep*. 2016;6:31599.
 67. Barratt HE, Budnick HC, Parra R, Lolley RJ, Perry CN, Nesic O. Tamoxifen promotes differentiation of oligodendrocyte progenitors in vitro. *Neuroscience*. 2016;319:146-154.
 68. Xu X, Bringas P Jr, Soriano P, Chai Y. PDGFR- α signaling is critical for tooth cusp and palate morphogenesis. *Dev Dyn*. 2005;232:75-84.
 69. Tallquist MD, Soriano P. Cell autonomous requirement for PDGFR α in populations of cranial and cardiac neural crest cells. *Development*. 2003;130:507-518.
 70. Dixon J, Jones NC, Sandell LL, et al. Tcof1/Treacle is required for neural crest cell formation and proliferation deficiencies that cause craniofacial abnormalities. *Proc Natl Acad Sci U S A*. 2006;103:13403-13408.
 71. Macintosh J, Michell-Robinson M, Chen X, Bernard G. Decreased RNA polymerase III subunit expression leads to defects in oligodendrocyte development. *Front Neurosci*. 2023;17:1167047.
 72. Lin Y, Pang X, Huang G, et al. Impaired eukaryotic translation initiation factor 2B activity specifically in oligodendrocytes reproduces the pathology of vanishing white matter disease in mice. *J Neurosci*. 2014;34:12182-12191.
 73. Duncan ID, Kondo Y, Zhang SC. The myelin mutants as models to study myelin repair in the leukodystrophies. *Neurotherapeutics*. 2011;8:607-624.
 74. Nave KA, Lai C, Bloom FE, Milner RJ. Jimpy mutant mouse: A 74-base deletion in the mRNA for myelin proteolipid protein and evidence for a primary defect in RNA splicing. *Proc Natl Acad Sci U S A*. 1986;83:9264-9268.
 75. Phillips RJ. Jimpy, a new totally sexlinked gene in the house mouse. *Z Indukt Abstamm Vererbungsl*. 1954;86:322-326.
 76. Sidman RL, Dickie MM, Appel SH. Mutant mice (quaking and jimpy) with deficient myelination in the central nervous system. *Science*. 1964;144:309-311.
 77. Perrier S, Michell-Robinson MA, Bernard G. POLR3-related leukodystrophy: Exploring potential therapeutic approaches. *Front Cell Neurosci*. 2021;14:631802.